Circulation
Arrhythmia and Electrophysiology
JOURNAL OF THE AMERICAN HEART ASSOCIATION

American Heart Association
Learn and Live

Multiple Potential Molecular Contributors to Atrial Hypocontractility Caused by Atrial Tachycardia Remodeling in Dogs

Reza Wakili, Yung-Hsin Yeh, Xiao Yan Qi, Maura Greiser, Denis Chartier, Kunihiro Nishida, Ange Maguy, Louis-Robert Villeneuve, Peter Boknik, Niels Voigt, Judith Krysiak, Stefan Kääb, Ursula Ravens, Wolfgang A. Linke, Gerrit J.M. Stienen, Yanfen Shi, Jean-Claude Tardif, Ulrich Schotten, Dobromir Dobrev and Stanley Nattel

Circ Arrhythm Electrophysiol 2010;3;530-541; originally published online July 26, 2010;
DOI: 10.1161/CIRCEP.109.933036
Circulation: Arrhythmia and Electrophysiology is published by the American Heart Association. 7272 Greenville Avenue, Dallas, TX 72514
Copyright © 2010 American Heart Association. All rights reserved. Print ISSN: 1941-3149. Online ISSN: 1941-3084

The online version of this article, along with updated information and services, is located on the World Wide Web at:
http://circep.ahajournals.org/content/3/5/530.full

Data Supplement (unedited) at:
http://circep.ahajournals.org/content/suppl/2010/07/26/CIRCEP.109.933036.DC1.html

Subscriptions: Information about subscribing to Circulation: Arrhythmia and Electrophysiology is online at
http://circep.ahajournals.org/site/subscriptions/

Permissions: Permissions & Rights Desk, Lippincott Williams & Wilkins, a division of Wolters Kluwer Health, 351 West Camden Street, Baltimore, MD 21201-2436. Phone: 410-528-4050. Fax: 410-528-8550. E-mail:
journalpermissions@lww.com

Reprints: Information about reprints can be found online at
http://www.lww.com/reprints

Downloaded from circep.ahajournals.org at Vrije on July 11, 2011

Multiple Potential Molecular Contributors to Atrial Hypocontractility Caused by Atrial Tachycardia Remodeling in Dogs

Reza Wakili, MD; Yung-Hsin Yeh, MD; Xiao Yan Qi, PhD; Maura Greiser, MD; Denis Chartier, BSc; Kunihiro Nishida, MD, PhD; Ange Maguy, PhD; Louis-Robert Villeneuve, MSc; Peter Boknik, MD; Niels Voigt, MD; Judith Krysiak, PhD; Stefan Kääb, MD; Ursula Ravens, MD; Wolfgang A. Linke, MD; Gerrit J.M. Stienen, MD; Yanfen Shi, MD; Jean-Claude Tardif, MD; Ulrich Schotten, MD, PhD; Dobromir Dobrev, MD*; Stanley Nattel, MD*

Background—Atrial fibrillation impairs atrial contractility, inducing atrial stunning that promotes thromboembolic stroke. Action potential (AP)-prolonging drugs are reported to normalize atrial hypocontractility caused by atrial tachycardia remodeling (ATR). Here, we addressed the role of AP duration (APD) changes in ATR-induced hypocontractility.

Methods and Results—ATR (7-day tachypacing) decreased APD (perforated patch recording) by ≈50%, atrial contractility (echocardiography, cardiomyocyte video edge detection), and $[Ca^{2+}]_i$ transients. ATR AP waveforms suppressed $[Ca^{2+}]_i$ transients and cell shortening of control cardiomyocytes; whereas control AP waveforms improved $[Ca^{2+}]_i$ transients and cell shortening in ATR cells. However, ATR cardiomyocytes clamped with the same control AP waveform had ≈60% smaller $[Ca^{2+}]_i$ transients and cell shortening than control cells. We therefore sought additional mechanisms of contractile impairment. Whole-cell voltage clamp revealed reduced I_{CaL}; I_{CaL} inhibition superimposed on ATR APs further suppressed $[Ca^{2+}]_i$ transients in control cells. Confocal microscopy indicated ATR-impaired propagation of the Ca^{2+} release signal to the cell center in association with loss of t-tubular structures. Myofilament function studies in skinned permeabilized cardiomyocytes showed altered Ca^{2+} sensitivity and force redevelopment in ATR, possibly due to hypophosphorylation of myosin-binding protein C and myosin light-chain protein 2a (immunoblot). Hypophosphorylation was related to multiple phosphorylation system abnormalities where protein kinase A regulatory subunits were downregulated, whereas autophosphorylation and expression of Ca^{2+}-calmodulin-dependent protein kinase IIδ and protein phosphatase 1 activity were enhanced. Recovery of $[Ca^{2+}]_i$ transients and cell shortening occurred in parallel after ATR cessation.

Conclusions—Shortening of APD contributes to hypocontractility induced by 1-week ATR but accounts for it only partially. Additional contractility-suppressing mechanisms include I_{CaL} current reduction, impaired subcellular Ca^{2+} signal transmission, and altered myofilament function associated with abnormal myosin and myosin-associated protein phosphorylation. The complex mechanistic basis of the atrial hypocontractility associated with AF argues for upstream therapeutic targeting rather than interventions directed toward specific downstream pathophysiological derangements. **(*Circ Arrhythm Electrophysiol*. 2010;3:530-541.)**

Key Words: atrial fibrillation ■ excitation contraction coupling ■ calcium ■ action potentials

Atrial fibrillation (AF) contributes significantly to the occurrence of stroke and other thromboembolic complications.[1] Atrial hypocontractility promotes the formation of left atrial thrombi that cause AF-related thromboembolic events.[1,2] AF-associated atrial tachycardia remodeling (ATR) reduces action potential (AP) duration (APD), and APD-

Clinical Perspective on p 541

Received December 18, 2009; accepted July 15, 2010.

From the Department of Medicine and Research Center (R.W., Y.-H.Y., X.Y.Q., D.C., K.N., A.M., L.R.V., Y.S, J.C.T., S.N.), Montreal Heart Institute and Université de Montréal, and Department of Pharmacology and Therapeutics (S.N.), McGill University, Montreal, Quebec, Canada; Department of Pharmacology and Toxicology (R.W., N.V., U.R., D.D.), Dresden University of Technology, Dresden, Germany; Division of Experimental Cardiology (N.V., D.D.), Department of Internal Medicine I, Medical Faculty Mannheim, University of Heidelberg, Heidelberg, Germany; Chang Gung Memorial Hospital (Y.-H.Y.) and Chang Gung University, Tao-Yuan, Taiwan; Department of Physiology (G.J.M.S.), VU Medical Center, Amsterdam, The Netherlands; Department of Pharmacology and Toxicology (P.B.), University of Münster, Münster, Germany; Department of Cardiovascular Physiology (J.K., W.A.L.), Ruhr University, Bochum, Germany; Department of Medicine I (R.W., S.K.), Klinikum Grosshadern, Ludwig-Maximilians University, Munich, Germany; and Department of Physiology (M.G., U.S.), University of Maastricht, Maastricht, The Netherlands.

*Drs Dobrev and Nattel share senior authorship.

The online-only Data Supplement is available at http:// circep.ahajournals.org/cgi/content/full/ CIRCEP.109.933036/DC1.

Correspondence to Stanley Nattel, MD, 5000 Belanger St E, Montréal, Quebec H1T 1C8, Canada. E-mail stanley.nattel@icm-mhi.org

© 2010 American Heart Association, Inc.

Circ Arrhythm Electrophysiol **is available at http://circep.ahajournals.org** **DOI: 10.1161/CIRCEP.109.933036**

Downloaded from circep.ahajournals.org at Vrije on July 11, 2011

prolonging drugs improve ATR-induced atrial hypocontractility.[3] APD is an important determinant of cellular Ca^{2+} loading and the systolic Ca^{2+} transient that triggers contraction. ATR decreases atrial cardiomyocyte Ca^{2+} transients, contributing to impaired cellular contractile function.[2] Reduced Ca^{2+} transients have been related to decreased cellular Ca^{2+} entry resulting from L-type Ca^{2+} current (I_{CaL}) downregulation by ATR,[2,4] but the marked APD shortening caused by ATR could itself account for reduced Ca^{2+} transients and hypocontractility.[3,5] Ca^{2+}-handling protein phosphorylation changes also occur in AF.[6] A recent study reported subcellular Ca^{2+}-handling abnormalities in atrial hypocontractility caused by chronic (over several months) AF.[7] However, short-term AF (over several days) can cause reversible atrial mechanical dysfunction and thromboembolic complications,[8] with apparent normalization by APD-prolonging drugs.[3] This study aimed to (1) evaluate the role of APD changes in hypocontractility induced by 1-week ATR, (2) determine whether APD changes alone were insufficient to account for contraction abnormalities, and (3) assess in detail other potential contributors.

Methods

This section includes essential methodologies. Additional details are found in the online-only Data Supplement.

Animal Model

All animal care and handling procedures were in accordance with National Institutes of Health guidelines (http://oacu.od.nih.gov/training/index.htm) and were reviewed and approved by the Animals Research Ethics Committee of The Montreal Heart Institute (Montréal, Quebec). Sixty-three adult mongrel dogs (22 to 36 kg) were divided into 2 groups: control (n=35) and 1-week ATR (n=28). Under diazepam (0.25 mg/kg IV), ketamine (5.0 mg/kg IV), and halothane (1% to 2%) anesthesia, unipolar leads were inserted into the right ventricular apex and right atrial (RA) appendage and connected to pacemakers in the neck. Atrioventricular block was created by radiofrequency ablation, and the right ventricle pacemaker was programmed to 80 bpm. After 24-hour recovery, the atrial pacemaker was programmed to pace the RA appendage at 400 bpm for 7 days.

On study days, dogs were anesthetized with morphine (2 mg/kg SC) and α-chloralose (120 mg/kg IV load at 29.25 mg/kg per hour) and ventilated mechanically. RA appendage effective refractory periods (AERPs) were determined with 8 basic stimuli followed by 1 premature stimulus (5-millisecond [ms] decrements). AF was induced multiple times by burst pacing to determine AF duration in each dog, and mean AF duration was calculated using average individual dog AF duration values.

Transthoracic echocardiography was performed under sedation (acepromazine 0.07 mg/kg and buprenorphine 0.009 mg/kg IM) in sinus rhythm. An average of 3 to 6 cardiac cycles was used, with the operator blinded to treatment assignment.

After open chest studies, hearts were excised through a median thoracotomy and immersed in oxygenated Tyrode solution. RA tissue was frozen in liquid N_2 for molecular biology. For cellular studies, RA preparations were coronary perfused at ≈10 mL/min for cardiomyocyte isolation. After perfusion with Ca^{2+}-free Tyrode-containing collagenase (110 U/mL) and 0.1% bovine serum albumin for ≈40 minutes, single cells were obtained by trituration. Cell capacitance averaged 102±4 picofarads and 101±5 picofarads in control and ATR cells, respectively.

Cellular Studies

Isolated cardiomyocytes were field stimulated through 10-ms 1.5×threshold square-wave pulses at a temperature of 35°C. Cell shortening, maximum contracting ($+\Delta L/\Delta t$), and relaxing ($-\Delta L/\Delta t$) slopes of cell shortening were measured by video edge detection based on the average of 10 consecutive beats. Cell shortening was measured during field stimulation with a video edge detector, with edge detection cursors positioned at both cell ends to measure whole-cell shortening. When AP clamp waveforms were applied through a patch pipette, absolute cell shortening was measured at only 1 cell end.

Cellular $[Ca^{2+}]_i$ transients were recorded with Indo-1 AM. Cells were excited with a 340-nm wavelength ultraviolet light. Emission ratios (400/500 nm) were used to calculate $[Ca^{2+}]_i$. Isolated cardiomyocytes from additional control and ATR dogs also were studied by confocal microscopy to analyze subcellular Ca^{2+} transient properties with Fluo-4 acetoxymethyl ester. For mean data analysis, 5 consecutive beats of each region of interest were averaged per cell and afterward per dog, allowing a comparison of lateral (longitudinal scans) or subsarcolemmal (transverse scans) to central Ca^{2+} transient amplitudes. Fluorescence intensity values were normalized to end-diastolic fluorescence intensity in regions of interest.

AP recordings were performed with whole-cell perforated patch techniques and current-clamp mode. Pipette tips were filled with nystatin-free intracellular solution by capillary action, and pipettes then were back filled with nystatin-containing (600 μg/mL) pipette solution. Whole-cell voltage clamp was performed with tight seal methods. Tip resistances were between 3 and 5 MΩ. Junction potentials averaged 15.9 mV and were corrected for AP recordings only. All recordings were performed at 35±0.5°C. In some experiments, mean control or ATR AP waveforms were applied as voltage-clamp command signals while recording Ca^{2+} transients or cell shortening. RA cardiomyocytes were subjected to typical AP waveforms from control and ATR cardiomyocytes at 2 Hz for sequential 6-minute periods (in randomized order). Parallel Ca^{2+} transients (10 to 20 beats) were recorded in 120-second intervals. For analysis, all Ca^{2+} transients obtained during the 6-minute periods were averaged and the mean±SEM calculated within each AP waveform group. For solution contents, see the online supplement.

Transverse Tubule Network Analysis

Freshly isolated atrial cells were plated on laminin-coated Petri dishes. Cells were labeled with 2-μmol/L di-4-ANEPPS in Tyrode solution. Samples were excited with an argon (488-nm) laser, and emitted fluorescence over 515-nm Z-series (250 nm) was acquired with an LSM 710 confocal microscope. The calculated point spread function of the imaging system was obtained with the use of 170-nm fluorescent latex beads. Acquired Z-series were deconvolved using maximum likelihood estimation with a Richardson-Lucy algorithm following gaussian prefiltering implemented with Huygens Professional 3.5.0. Projections were analyzed by excluding the cell membrane and quantifying intracellular membrane staining. Transverse tubule (t-tubule) density was estimated from the pixel intensity normalized to the surface area of the intracellular region for each cardiomyocyte.

Skinned Cardiomyocyte Studies

Cardiomyocytes were mechanically isolated, permeabilized, and mounted. Isometric force measurements were performed at 15°C and resting sarcomere length of 2.2 μm. Force redevelopment rate (K_{TR}) was determined during activation at different Ca^{2+} concentrations. Force redevelopment after restretch was fitted by a single exponential function (Marquart-Levenberg algorithm) to estimate K_{TR}. Passive force was determined in relaxing solution by applying the same shortening (20% of original cell length) followed by a restretch after 10 seconds.

Protein Studies

RA tissue homogenates were prepared from freeze-dried tissue, and protein concentrations were determined with Amido-black

Downloaded from circep.ahajournals.org at Vrije on July 11, 2011

Table 1. In Vivo Hemodynamic and Electrophysiological Data

	Control (n=16)	ATR (n=16)
Systolic BP, mm Hg	132±5	128±3
Diastolic BP, mm Hg	82±4	80±2
LVEDP, mm Hg	4.9±0.5	4.5±0.4
RAP, mm Hg	2.7±0.5	2.6±0.4
AERP (BCL 360 ms), ms	126±5	70±3*
AERP (BCL 300 ms), ms	123±4	68±2*
AERP (BCL 250 ms), ms	118±4	68±3*
AERP (BCL 200 ms), ms	113±4	70±3*
AERP (BCL 150 ms), ms	102±4	70±2*
DAF, s	26±6	324±56†

Data are presented as mean±SEM. BCL indicates basic cycle length; BP, blood pressure; DAF, duration of AF; LVEDP, LV end-diastolic pressure; RAP, RA mean pressure.

*$P<0.001$ versus control.

†$P<0.01$ versus control.

10B. Proteins were fractionated on SDS-PAGE and transferred to nitrocellulose membranes. Protein expression was quantified as previously described.[6] For details regarding antibodies, dilution, and source, see the online supplement. Serine and threonine protein phosphatase activity were assessed with phosphorylase-A as substrate and quantified as nanomoles of $^{32}P_i$ released/mg protein per minute. Differentiation between type 1 and type 2A protein phosphatase (PP1 and PP2A, respectively) activities was obtained with okadaic acid (3 nmol/L). Protein bands were visualized with electrochemoluminescence reagents and Hyperfilm-ECL. The films were evaluated densitometrically with Phoretix 1D software. Myosin heavy chain (MHC) isoform composition was analyzed by 1D SDS-PAGE. The separating gel contained 12% total acrylamide (acrylamide-to-bis-acrylamide ratio, 200:1; pH 9.3), whereas the stacking gel contained 3.5% total acrylamide (acrylamide-to-bis-acrylamide ratio, 20:1; pH 6.8). Gels were silver stained and analyzed by laser densitometry. To check for linearity, different amounts of protein were loaded on the gels, and band densities were determined. Only samples within the linear range (typically 0.2 to 1.0 μg of total protein) were used in the evaluation. Agarose-strengthened 2% SDS-PAGE was used to detect titin.

Data Analysis

Skinned cardiomyocyte force-pCa relations were fit with the use of a nonlinear procedure by the Hill equation: $F(Ca^{2+})/F_{max}=[Ca^{2+}]^{nH}/(Ca_{50}{}^{nH}+[Ca^{2+}]^{nH})$, where F denotes the steady-state force; F_{max}, active isometric force at saturating Ca^{2+} concentrations (Marquart-Levenberg algorithm); and nH, Hill coefficient, indicating steepness of the force-pCa relation.

All data are presented as mean±SEM. For single comparisons, paired or nonpaired *t* tests were applied as appropriate. Repeated-measures analyses were performed with 2-way ANOVA. When significant interactions were found between main effects, Bonferroni-corrected *t* tests were applied to determine the levels of the repeated measures at which significant differences occurred (the *P* values shown were obtained by multiplying each *P* by the number of repeated tests performed). In the absence of interaction, the significance of main effects differences is shown. Analyses of nonrepeated measurements in multiple groups (control versus 24-hour recovery versus 48-hour recovery) were performed by 1-way ANOVA followed (if significant) by the least significant difference test. The specific statistical test applied for each analysis is provided in the online supplement. A 2-tailed $P<0.05$ was considered statistically significant.

The authors had full access to the data and take responsibility for its integrity. All authors have read and agree to the manuscript as written.

Results

In Vivo Experiments

All ATR dogs showed atrial remodeling, with significantly reduced AERPs and AERP rate adaptation (Table 1). Arterial pressures, left ventricular (LV) end-diastolic pressure, and RA pressure were unchanged by ATR. ATR significantly increased the duration of burst pacing-induced AF, an index of the AF-maintaining substrate, by ≈10-fold ($P<0.001$). Echocardiography revealed atrial contractile dysfunction in ATR (Figure 1A and B). Overall, atrial fractional area and

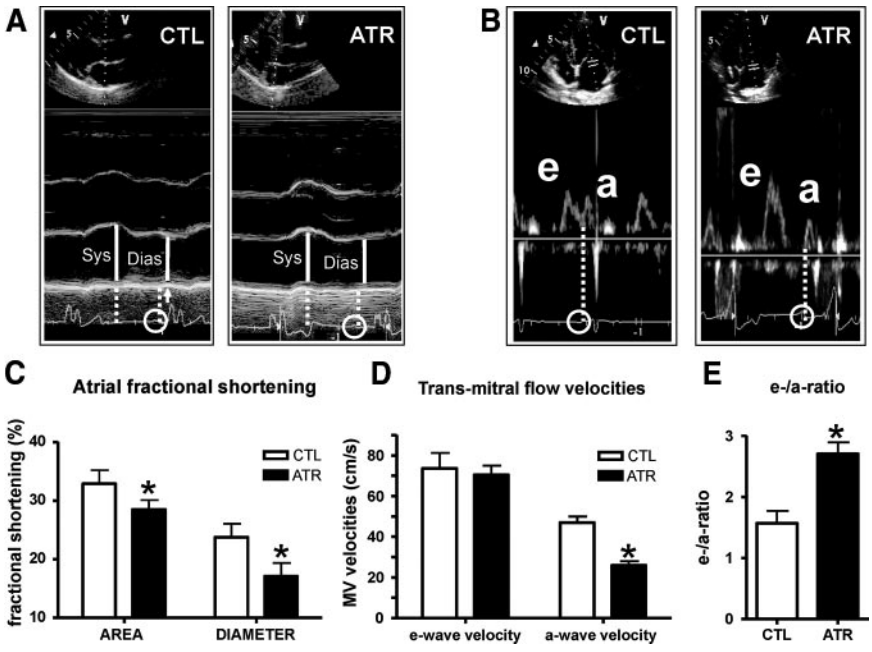

Figure 1. A, Representative M-mode echocardiographic images showing the left atrial (LA) dimension at end-systole and diastole. B, Pulsed-wave Doppler recording at the mitral valve, with E- and A-waves shown. Circles indicate P-waves preceding active atrial contraction. C to E, Mean±SEM echocardiographic results of atrial fractional shortening of LA area and LA diameter (C), mitral valve velocities at E- and A-wave (D), and E/A ratio (E) in control and ATR dogs (n=8 for both groups). CTL indicates control; Dias, diastole; Sys, systole. *$P<0.05$.

Downloaded from circep.ahajournals.org at Vrije on July 11, 2011

Table 2. Echocardiographic LV Data

	Control (n=5)	ATR (n=7)
LVVd, mL	42.9±6.4	46.7±3.0
LVVs, mL	17.8±4.1	19.3±2.2
EF, %	60.0±3.6	58.9±3.2

Data are presented as mean±SEM. There were no statistically significant intergroup differences. EF indicates ejection fraction; LVVd, left ventricular volume diastolic; LVVs, LV volume systolic.

diameter shortening were decreased by ≈14% ($P<0.05$) and ≈26% ($P<0.05$), respectively (Figure 1C). Mitral valve A-wave velocity (representing active atrial contractile function) was decreased by ≈45% in ATR ($P<0.05$) (Figure 1D), whereas E-wave velocity (representing passive atrial emptying function) was unchanged. The E/A ratio was nearly doubled by ATR (2.7±0.2) versus control (1.6±0.2; $P<0.05$) (Figure 1E). LV dimensions and ejection fraction were unchanged (Table 2).

Cell Shortening, Ca^{2+} Transients, and APD

Figure 2A shows representative cell shortening recordings at 1 Hz. Overall cell shortening was strongly reduced by ≈85% ($P<0.001$) in ATR cardiomyocytes versus control cells (Figure 2B). ATR decreased cell shortening over a wide range of frequencies ($P<0.001$) (supplemental Figure 1). Absolute cell shortening and relaxation rates were substantially reduced in ATR ($+\Delta L/\Delta t$ and $-\Delta L/\Delta t$ by 81% and 93%, respectively; $P<0.001$ for each) (Figure 2C).

Figure 2D shows representative steady-state Ca^{2+} transient recordings. ATR decreased Ca^{2+} transient amplitudes over a wide range of frequencies, flattening Ca^{2+} transient frequency dependence (Figure 2E). Diastolic $[Ca^{2+}]_i$ levels were unchanged (supplemental Figure 2). To assess sarcoplasmic reticulum (SR) Ca^{2+} content, we measured caffeine-evoked Ca^{2+} transients as illustrated in Figure 3A. Overall data (Figure 3B) show ≈30% decreases ($P<0.05$) in caffeine-evoked Ca^{2+} transients in ATR. Ca^{2+} transient decay was accelerated (time constant, 782±40 ms) versus control (1325±63 ms; $P<0.01$), suggesting increased forward mode Na^+, Ca^{2+} exchange function (Figure 3C). These results point to reduced SR-derived Ca^{2+} transients associated with reduced SR Ca^{2+} stores as a basis for hypocontractility, consistent with prior observations.[2]

We then recorded AP waveforms. Ca^{2+} entry occurs predominantly during the AP plateau where changed plateau voltages and durations affect SR Ca^{2+} loading[9] and could explain ATR-induced hypocontractility.[3] Figure 3D shows representative AP recordings. ATR abbreviated APD over a wide range of frequencies by ≈50% overall ($P<0.001$) (Figure 3E).

Contribution of AP Waveform Changes to Reduced Ca^{2+} Transients

Mean AP waveforms obtained in control and ATR cells at 2 Hz were applied to individual control cells at 2 Hz during Ca^{2+} transient or cell shortening recording. Representative Ca^{2+} transients in 1 control cell are shown in Figure 4A. The ATR waveform clearly reduced Ca^{2+} transients. Overall, clamping control cells with ATR APs caused a ≈45% decrease ($P<0.05$) in Ca^{2+} transient amplitude (Figure 4B). We then used the same approach to study the impact of APD abbreviation on cell shortening in AP-clamped control cells. The ATR AP waveform also substantially reduced cell shortening (Figure 4C, left) by ≈75% overall ($P<0.001$) (Figure 4C, right).

If the AP waveform changes induced by ATR are the sole cause of cell Ca^{2+} and contractile abnormalities, it should be possible to normalize Ca^{2+} transients and cell shortening by applying control waveforms to ATR cells. Ca^{2+} transient recordings from an ATR cell exposed to control and ATR waveforms are shown in Figure 4D. The control AP waveform improved the Ca^{2+} transient; overall, Ca^{2+} transient amplitudes were approximately doubled ($P<0.05$) in ATR cells when control waveforms were applied (Figure 4E). Nevertheless, comparing the recordings in Figure 4D with control cell recordings in Figure 4A and mean data in Figure

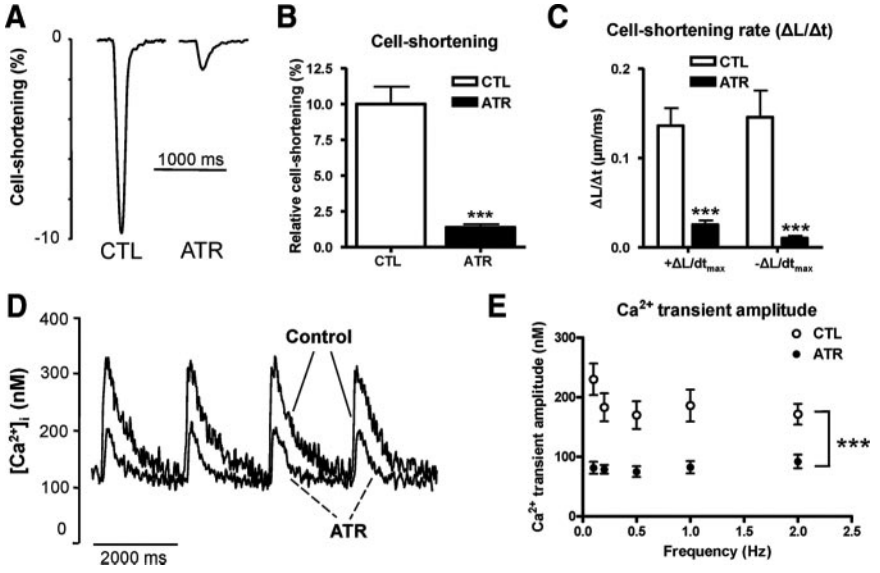

Figure 2. A, Representative recordings of cell shortening during 1-Hz field stimulation from single CTL and ATR cardiomyocytes. B, Corresponding mean±SEM data (n=13 and n=17 cells for CTL and ATR, respectively). ***$P<0.001$ for CTL versus ATR. C, Mean±SEM cell shortening kinetics ($+\Delta L/\Delta t$ for contraction and $-\Delta L/\Delta t$ relaxation) at 1-Hz stimulation in CTL versus ATR cardiomyocytes (n=13 and n=17 for CTL and ATR, respectively). ***$P<0.001$. D, Original recordings of Ca^{2+} transients during 0.5-Hz stimulation. E, Mean±SEM Ca^{2+} transient amplitude as function of stimulation frequency (n=25 and 15 cells for CTL and ATR, respectively). ***$P<0.001$ for effect of group. CTL indicates control.

Downloaded from circep.ahajournals.org at Vrije on July 11, 2011

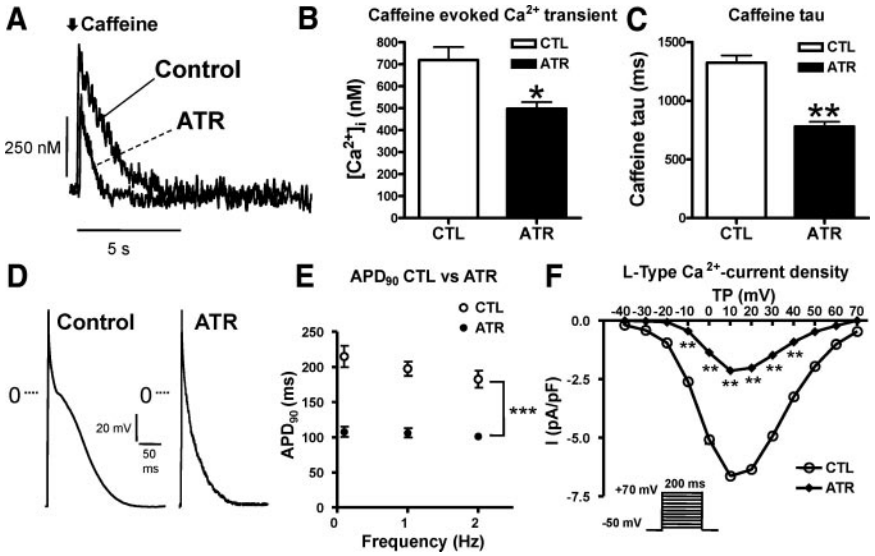

Figure 3. A, Examples of caffeine-induced Ca^{2+} transients in CTL and ATR cardiomyocytes. A 10-mmol/L local caffeine concentration was achieved in <500 ms with a laminar flow rapid solution switching system. B, Mean±SEM caffeine-evoked Ca^{2+} transient amplitudes (n=17 and n=23 cells for CTL and ATR, respectively). *P<0.05. C, Mean±SEM Ca^{2+} decay time constant (tau) of caffeine-induced Ca^{2+} transients (n=17 and n=23 cells for CTL and ATR, respectively). **P<0.01. D, Examples of AP waveforms obtained at 1-Hz stimulation. E, Mean±SEM APD_{90} at different pacing frequencies (n=12 and 10 cells for CTL and ATR, respectively). ***P<0.001 for CTL versus ATR, effect of group. F, Mean±SEM I_{CaL} density as a function of test potential (n=11 cells for each group). **P<0.01. APD_{90} indicates APD at 90%; TP indicates test potential.

4E with control cell data in Figure 4B, the control AP waveform did not normalize Ca^{2+} transients in ATR cells. For example, Ca^{2+} transient amplitudes in control cells clamped with a control AP waveform averaged 147±33 nmol/L, whereas ATR cells clamped with the same waveform had Ca^{2+} transient amplitudes of 61±5 nmol/L (P<0.05). Similar results were obtained for contractility changes. The control AP waveform significantly improved contractility in ATR cells (Figure 4F) but clearly did not return cell shortening to control (compare to Figure 4C); control cell shortening averaged 5.9±1.0 μm with the control AP waveform versus 2.4±0.3 μm in ATR cells clamped with the control AP waveform (P<0.01). These results confirm a role of ATR-induced AP waveform changes in Ca^{2+} release and contractile abnormalities but indicate that only a minority of the changes are attributable to APD abbreviation. We therefore examined additional potential contributors to ATR-induced Ca^{2+} transient reduction and hypocontractility.

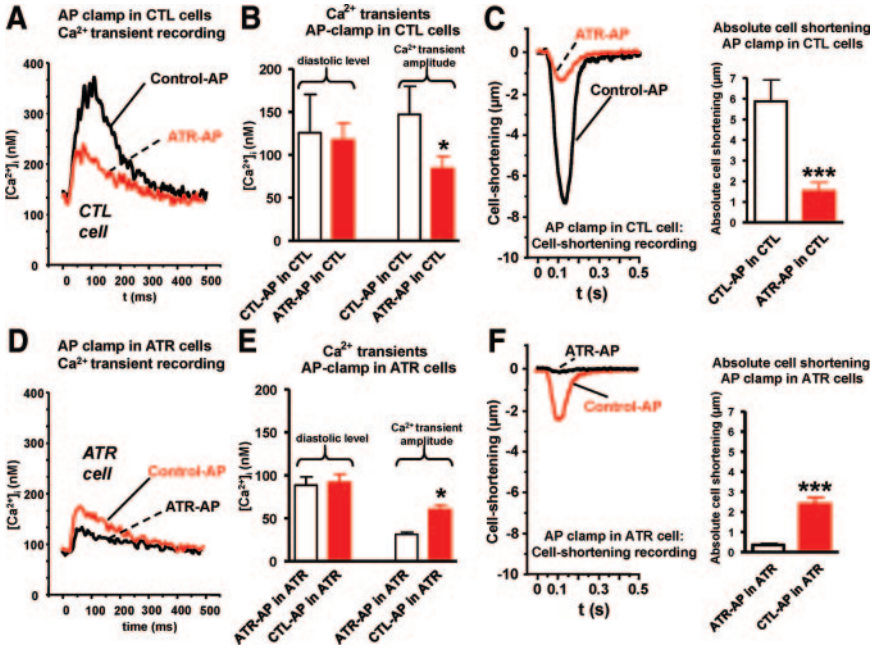

Figure 4. AP clamp results (all data obtained with mean AP waveforms obtained in current-clamp mode at 2 Hz and applied to other cells in voltage-clamp mode at 2 Hz). A, Ca^{2+} transient recordings obtained from a single CTL cell during application of typical CTL (black) or ATR (red) AP-waveform. B, Mean±SEM diastolic Ca^{2+} levels and Ca^{2+} transient amplitudes obtained with AP clamp in CTL cells (n=5). *P<0.05 for CTL AP versus ATR AP. C, Cell-shortening elicited by AP clamp in CTL (left, original cell shortening recordings from a single CTL cell subjected to typical CTL [black] or ATR [red] AP waveforms; right, mean±SEM cell shortening during AP clamp in CTL cells) (n=8). ***P<0.001 for ATR AP versus CTL AP. D, Ca^{2+} transient recordings obtained from a single ATR cell during application of typical CTL (red) or ATR (black) AP waveforms. E, Mean±SEM diastolic Ca^{2+} levels and Ca^{2+} transient amplitudes obtained with AP clamp in ATR cells (n=7). *P<0.05 for CTL AP versus ATR AP. F, Cell shortening elicited by AP clamp in ATR (left, original cell shortening recording from a single ATR cell subjected to typical CTL [red] or ATR [black] AP waveforms; right, mean±SEM cell shortening during AP clamp in ATR cells) (n=7). ***P<0.001 for ATR AP versus CTL AP. CTL indicates control.

Downloaded from circep.ahajournals.org at Vrije on July 11, 2011

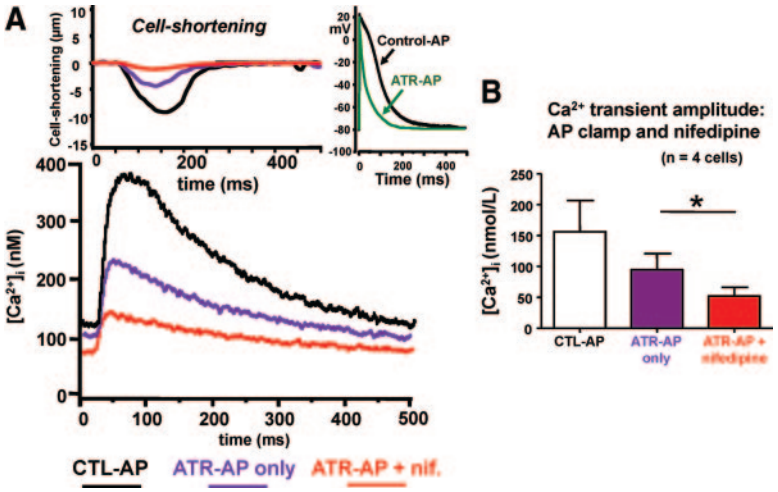

Figure 5. AP-clamp experiments to study role of I_{CaL} changes independent of APD. All data were obtained with mean AP waveforms based on all current-clamp recordings at 2 Hz. A, Top left shows mean CTL AP waveform (black) and ATR AP waveform (green) applied in voltage-clamp mode at 2 Hz. The bottom shows Ca^{2+} transient recordings obtained from a single CTL cell during application of typical CTL (black) or ATR (purple) AP waveform and during ATR AP waveform and perfusion with 5-μmol/L nifedipine (red). The top left shows corresponding cell shortening recordings from a CTL cell subjected to CTL (black) or ATR (purple) AP waveforms and during ATR AP waveform and perfusion with nifedipine (red). B, Mean±SEM Ca^{2+}transient amplitudes obtained with AP clamp in CTL cells (n=4). *$P<0.05$ for ATR AP+nifedipine versus ATR AP alone. CTL indicates control; Nif, nifedipine.

I_{CaL} Changes

Previous studies have shown important I_{CaL} downregulation in ATR,[4,10,11] and I_{CaL} is the major source of Ca^{2+} entry for SR Ca^{2+} loading.[9] For a given AP waveform, decreased I_{CaL} channel function would be expected to diminish cellular Ca^{2+} loading by virtue of reduced Ca^{2+} entry through the L-type channel. Figure 3F shows mean I_{CaL} density-voltage relations in ATR and control cells obtained with 10 mmol/L EGTA-containing pipettes. I_{CaL} was significantly reduced (−68%; $P<0.01$ at all test potentials between −10 and +40 mV) in ATR cells, consistent with previous results.[4,10,11] I_{CaL} kinetics and voltage dependence were unchanged (supplemental Figure 3). These data may not accurately reflect physiological I_{CaL} changes because reduced Ca^{2+} transients in ATR cells should decrease $[Ca^{2+}]_i$-dependent I_{CaL} inactivation, which would not be reflected in 10-mmol/L EGTA-buffered cells. We therefore repeated the I_{CaL} measurements with EGTA-free pipette solution. Supplemental Figure 4A shows representative I_{CaL} recordings, and Figure 4B shows corresponding current density-voltage relations. Overall, peak I_{CaL} density was reduced by 63% in ATR cells ($P<0.001$ at all test potentials between −10 and +40 mV). In contrast to findings with EGTA-containing pipettes, fast inactivation time constants were significantly slowed ($P<0.001$) (supplemental Figure 5A), consistent with reduced Ca^{2+}-dependent I_{CaL} inactivation. Slow I_{CaL} inactivation kinetics (supplemental Figure 5B) and I_{CaL} voltage dependence (supplemental Figure 5C) were unaltered by ATR under EGTA-free conditions, but recovery was accelerated ($P<0.01$) (supplemental Figure 5D).

To assess whether decreased Ca^{2+} entry through I_{CaL} reduces Ca^{2+} transients over and above the APD abbreviation caused by ATR, we recorded Ca^{2+} transients in control cells subjected to AP clamping with control APs, ATR APs, and then ATR APs in the presence of 5 μmol/L nifedipine. Figure 5A shows representative Ca^{2+} transients. ATR APs reduced Ca^{2+} transients versus control APs, but when nifedipine was added to suppress Ca^{2+} current, Ca^{2+} transients were further decreased for the same ATR APs. The top left shows corresponding cell shortening. Cell contraction changes paralleled those in Ca^{2+} transients. Mean Ca^{2+} transient data (Figure 5B) indicate that decreasing I_{CaL} significantly reduces Ca^{2+} transients over and above changes produced by ATR AP alterations ($P<0.05$).

Expression and Phosphorylation of Key Ca^{2+}-Handling Proteins

To uncover potential contributions of altered Ca^{2+}-handling protein expression to Ca^{2+}-handling abnormalities, we performed Western blots with specific antibodies directed against total and phosphorylated forms of target proteins. We found no significant differences between ATR and control atria in SR-associated proteins (supplemental Figure 6). Expression levels of total ryanodine receptor 2 (RyR2), protein kinase A (PKA)-phosphorylated RyR2 (at Ser2809), Ca^{2+}-calmodulin-activated protein kinase (CaMKII)-phosphorylated RyR2 (at Ser2815), and fractional RyR2-phosphorylation states (ratios of Ser2809-RyR2 and Ser2815-RyR2 to total RyR2) were similar in control and ATR cells (supplemental Figure 6A). Calsequestrin-2, the major SR Ca^{2+} buffer system protein, was similarly unaffected by ATR, as were SR Ca^{2+} ATPase and Na^+,Ca^{2+} exchange 1 (supplemental Figure 6B). No significant changes were noted for total phospholamban (PLB) or for PKA-phosphorylated (at Ser16) or CaMKII-phosphorylated (at Thr17) PLB.

Subcellular Ca^{2+} Handling

Recent studies have emphasized the importance of subcellular Ca^{2+}-handling abnormalities in rabbits with ATR[12] and sheep with long-standing AF or heart failure.[7,13] We assessed this possibility in control and ATR cardiomyocytes with the use of confocal microscopy. Longitudinal line scans showed no significant change in cells from ATR dogs compared with controls (supplemental Figure 7). Ca^{2+} transient signals were reduced in ATR cells but uniformly along the length of the cell. In contrast, transverse line scans showed substantial alterations (Figure 6). Whereas under control conditions, subsarcolemmal and central cellular Ca^{2+} signals were similar (Figure 6A), in ATR cells, central Ca^{2+} transients were delayed and reduced in amplitude compared to subsarcolemmal signals ($P<0.001$), indicating impaired Ca^{2+} signal

Downloaded from circep.ahajournals.org at Vrije on July 11, 2011

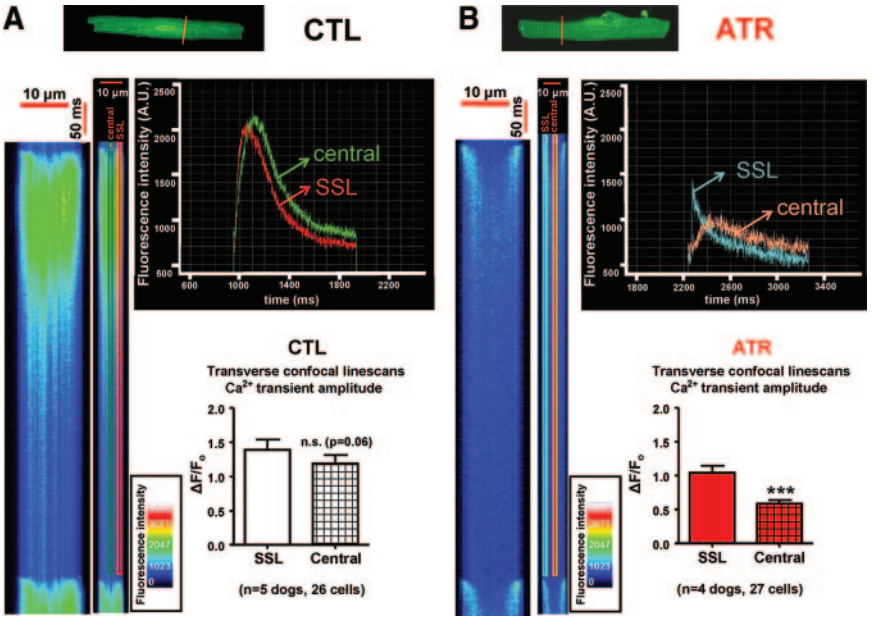

Figure 6. Transverse distribution of Ca^{2+} fluorescence in CTL and ATR cells. A, CTL group results. An image illustrating the scan direction is shown along with the corresponding line scan image (stimulation frequency, 1 Hz) and a smaller image showing regions of interest (central and SSL) with corresponding original Ca^{2+} transient recordings. Also shown, CTL group mean±SEM data for SSL versus central Ca^{2+} transients. B, ATR group results and ATR group mean±SEM data (n=5 dogs/group). ***$P<0.001$ for SSL versus central Ca^{2+} transients. CTL indicates control; SSL, subsarcolemmal.

propagation toward the center of the cell (Figure 6B). Confocal imaging with di-4-ANEPPS indicated the presence of t-tubular structures under control conditions, which were greatly reduced in ATR cells (supplemental Figure 8A). Overall, t-tubule density was decreased by ≈60% in ATR ($P<0.01$) (supplemental Figure 8B).

Force Development in Permeabilized Cardiomyocytes

To investigate whether abnormal myofibrillar behavior may contribute to atrial contractile dysfunction, we assessed myofilament mechanics by recording force development in skinned permeabilized cardiomyocytes (Figure 7A). Passive and active force development and K_{TR} were measured in 18 cardiomyocytes from 5 ATR dogs and 19 cardiomyocytes from 5 control dogs. Figure 7B shows a recording of isometric force development in an ATR cardiomyocyte at saturating Ca^{2+} (pCa 4.5). Overall data are presented in Figure 7C. Passive force per cross-sectional area were not different in ATR (1.69±0.17 kN/m^2) versus control cells (1.94±0.33 kN/m^2; P=NS). Maximal Ca^{2+}-activated isometric force per cross-sectional area also were comparable (ATR, 27.71±1.75 kN/m^2; control, 31.65±3.49 kN/m^2; P=NS). Average force-pCa relationships are shown in Figure 7D. The pCa_{50} values were slightly, but significantly, higher in ATR (5.49±0.01) versus control (5.46±0.02; $P<0.001$), indicating increased Ca^{2+} responsiveness in ATR. The steepness of the force-pCa relation (nH) was not different (ATR, 3.94±0.16; control, 4.24±0.27). The K_{TR} (measured at pCa 4.5) was significantly slower (by ≈20%) in ATR (3.74±0.30 seconds^{-1}) versus control (4.72±0.30 seconds^{-1}; $P<0.05$), suggesting altered cross-bridge kinetics (Figure 7D, right).

Expression and Phosphorylation of Key Myofilament Proteins

We analyzed expression changes in important myofilament proteins as a potential contributor to contractile abnormalities. Expression levels of thin myofilament proteins troponin (Tn)I and TnC are shown in Figure 8A. Total TnI expression, PKA-phosphorylated (at Ser23/24) TnI, the phosphorylated/total TnI ratio, and total TnC were unchanged by ATR. Thick myofilament and myosin-related protein results are presented in Figure 8B. Total protein levels of thick myofilament myosin-binding protein-C (MyBP-C) were unchanged. However, PKA-phosphorylated MyBP-C (at Ser282) was significantly decreased in ATR by ≈35% ($P<0.05$), resulting in a decreased Ser282-MyBP-C/total MyBP-C ratio ($P<0.05$). Reduced MyBP-C phosphorylation could contribute to alterations in cross-bridge kinetics. Myosin light chain (MLC) kinase phosphorylation of MLC protein-2a (MLC2a) at Ser21/22 is suggested to improve atrial contractility by improving cross-bridge cycling kinetics,[14] and we found a ≈30% reduction in MLC2a phosphorylation in ATR ($P<0.05$) (Figure 8B). Contractile protein composition was determined by 1D SDS-PAGE (supplemental Figure 9). The detail of the MHC region shown in Figure 8C illustrates the presence of 2 MHC-isoforms, fast (α) and slow (β), in atrial tissue. The quantity of α-MHC as a percentage of total ($\alpha+\beta$) MHC content was not affected by ATR. The expression of titin, a giant protein that acts as a molecular spring in the I-band, is anchored at the Z-disk, and is expressed in 2 main cardiac isoforms (a longer, more-compliant N2BA titin [3.3 to 3.5 MDa] and a shorter, stiffer N2B titin [3.0 MDa]) was unchanged in ATR (Figure 8D). Overall, the myofilament analyses point to dephosphorylation of MyBP-C and MLC2a as potential contributors to ATR-induced myofilament dysfunction.

Phosphorylation Changes, Kinases, and Phosphatases

To identify potential sources of altered myofilament protein phosphorylation, we analyzed the expression of PP1 and PP2A and of PKA and CaMKII (supplemental Figure 10). In

Downloaded from circep.ahajournals.org at Vrije on July 11, 2011

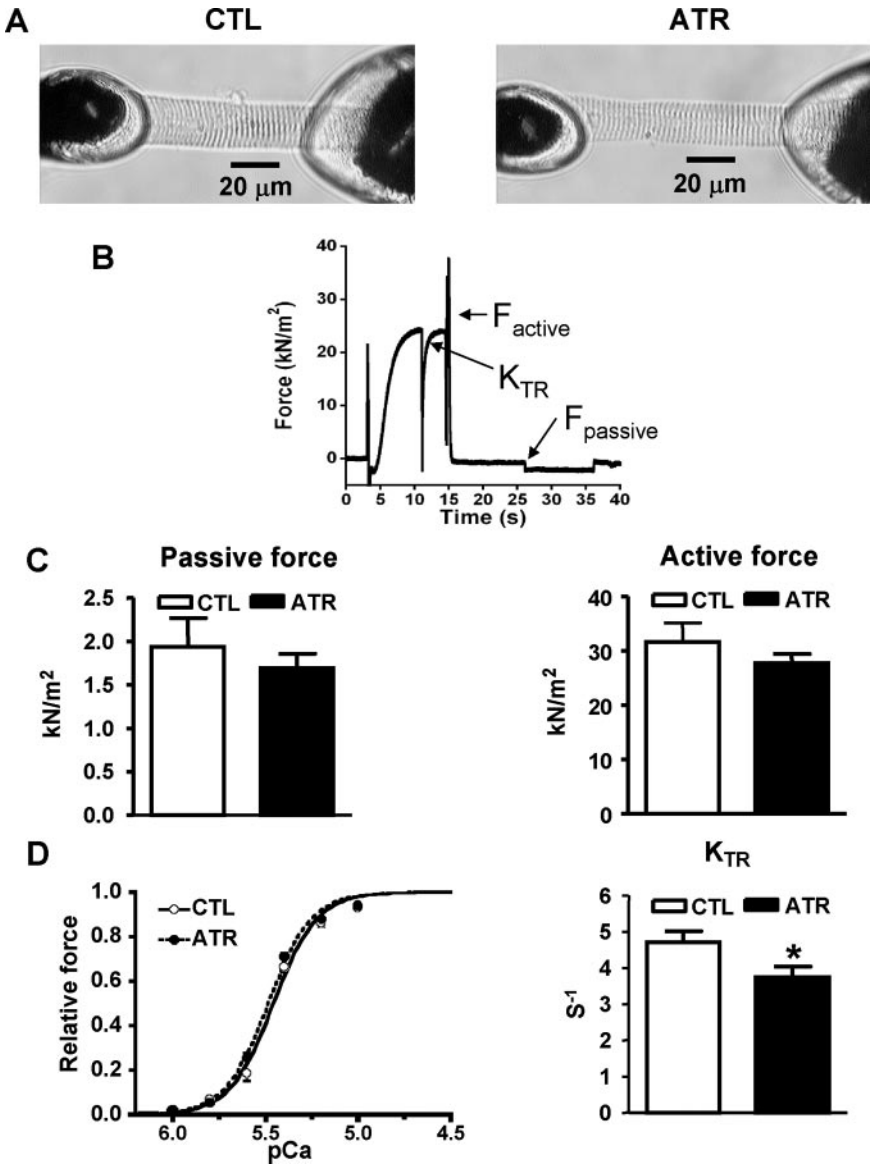

Figure 7. A, Images of a single permeabilized cardiomyocyte from a CTL and an ATR dog mounted in the experimental setup between force transducer and piezoelectric motor. B, Example of force recording. Contraction-relaxation sequence recorded from a cardiomyocyte at maximally activating Ca^{2+} concentration (pCa 4.5). Slack test used to determine the K_{TR}. C, Passive force at pCa 9.0 and maximum force pCa 4.5 expressed per cross-sectional area in both groups. D, Isometric force as a function of the pCa of the activating solution, normalized to the force at saturating Ca^{2+} concentration and maximum K_{TR} in CTL and ATR. *$P<0.05$ versus CTL. CTL indicates control.

addition, we directly measured PP enzyme activity. Total (PP1+PP2A) and PP2A-related activities were comparable in both groups, whereas PP1 activity was 28% greater in ATR ($P<0.05$) (supplemental Figure 10A). The increased PP1 activity was not attributable to expression differences (supplemental Figure 10B). PKA expression was unchanged for PKAc (the catalytic subunit), whereas the regulatory subunit $PKA_{II\alpha}$ was decreased by 33% ($P<0.05$) (supplemental Figure 10C). ATR increased the expression and autophosphorylation of the cytosolic CaMKIIδ isoform by 78% and 123%, respectively ($P<0.05$ for each), whereas the ratio of autophosphorylated CaMKIIδ to total CaMKIIδ was unchanged (P=NS) (Figure 8D). The increase in PP1 activity and decrease in $PKA_{II\alpha}$ protein expression, consistent with previous data,[6,15] potentially account for the observed myofilament protein dephosphorylation. Increased PP1 activity may have offset the increased expression of the cytosolic CaMKIIδ isoform, explaining the lack of changes in CaMKII phosphorylation of investigated proteins.

Recovery of ATR-Induced Electrophysiological and Contractile Alterations

To analyze the relationship between electric and contractile changes during ATR recovery, we studied dogs (5 per group) subjected to 7-day ATR followed by a 24- or 48-hour nonpaced recovery interval as well as 5 concurrent controls. The results are summarized in Table 3. After 24-hour recovery, significant decreases remained for APDs recorded over a wide range of frequencies ($P<0.01$) (supplemental Figure 11A), Ca^{2+} transients ($P<0.01$) (supplemental Figure 11B), and cell-shortening ($P<0.001$) (supplemental Figure 11C). In contrast, full recovery was seen for all indices at 48 hours (P=NS versus control).

Discussion

In the present study, we observed that 7 days of ATR are sufficient to substantially impair atrial contractile function. A significant part of the contractile abnormality can be attributed to AP changes caused by ATR, but even when these are

Downloaded from circep.ahajournals.org at Vrije on July 11, 2011

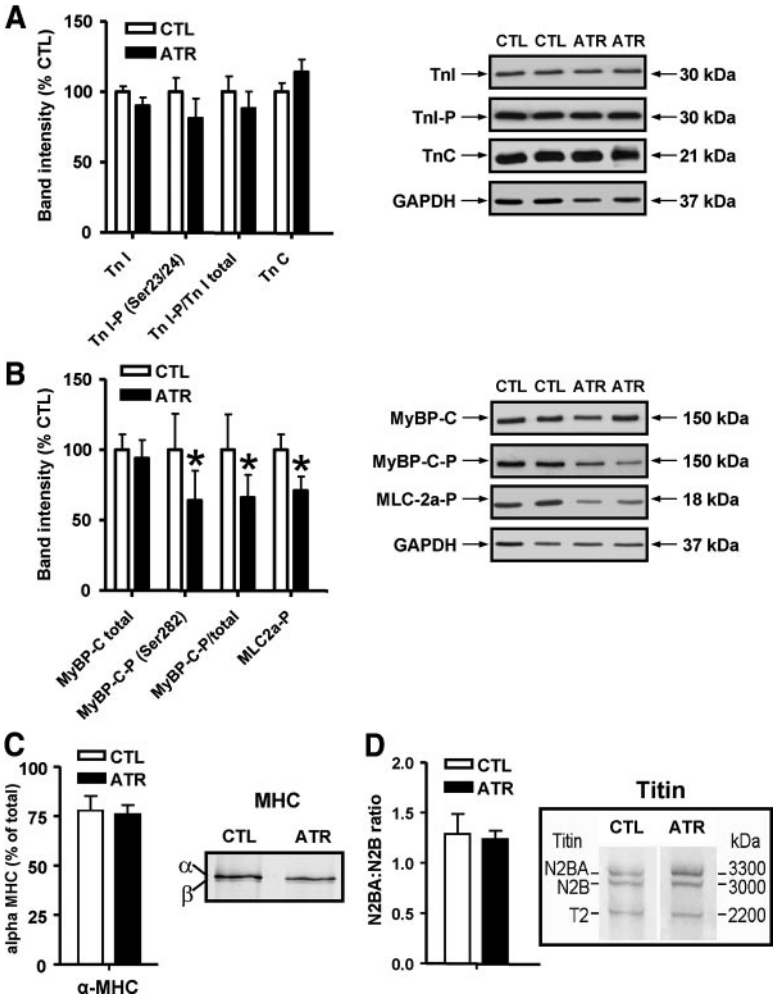

Figure 8. Protein expression data (mean±SEM band intensities normalized to GAPDH and expressed relative to CTL) and corresponding illustrative examples (right). A, TnI, Ser23/24 TnI-P, and TnC with corresponding GAPDH bands (CTL, n=10; ATR, n=8 atria/analysis). B, Total MyBP-C, Ser282 MyBP-C-P, and PKA MLC2a-P with corresponding GAPDH bands (CTL, n=14; ATR, n=10 atria/analysis). *$P<0.05$ versus CTL. C, MHC isoform composition (mean±SEM values for α MHC expression as a percentage of total ($\alpha+\beta$) MHC expression) and detail of the MHC region of an SDS-PAGE illustrating the similarity in MHC expression in the 2 groups (right). D, Titin N2BA and N2B isoforms separated by 2% SDS-PAGE (N2BA:N2B ratio mean±SEM; n=10 atria/group per analysis; P=NS ATR versus CTL). CTL indicates control; MLC2a-P, phosphorylated MLC2a; MyBP-C-P, phosphorylated MyBP-C; T2, titin degradation band; TnI-P, phosphorylated TnI.

accounted for, substantial abnormalities in atrial Ca^{2+} release and contractility remain. Detailed analyses point to loss of I_{CaL} as a significant additional contributor along with potential roles for disturbed subcellular distribution of Ca^{2+} release and intrinsic myofilament dysfunction likely caused by myosin and myosin-associated protein dephosphorylation.

Previous Studies of Atrial Hypocontractility Mechanisms

It has long been recognized that AF causes atrial hypocontractility,[16] and the role of atrial contractile dysfunction in the thromboembolic complications of AF is well appreciated.[8] Even very short-term AF (5 to 15 minutes) can cause contractile dysfunction, but normal contraction resumes within minutes of rhythm reversion after such brief episodes, whereas persistent hypocontractility (lasting ≥24 hours) follows AF episodes lasting days to weeks.[8] Atrial tachypaced dogs with uncontrolled ventricular responses show an atrial cardiomyopathic phenotype, with contractile dysfunction related to reduced Ca^{2+} transients of uncharacterized mechanism.[2] In atrial tissue samples from patients with AF, contractile force is impaired and can be normalized by increasing extracellular Ca^{2+} but not by exposure to a Ca^{2+} channel agonist, again suggesting a primary role for reduced Ca^{2+} load.[5]

Table 3. Data Following ATR Recovery Versus Parallel Control Dogs

	Control (n=5)	ATR Recovery 24 h (n=5)	ATR Recovery 48 h (n=5)
APD_{90} at 1 Hz, ms	220±14	163±12*	207±11
$[Ca^{2+}]_i$ transient, nM	192±10	131±12†	183±11
Cell shortening, %	11.2±0.3	5.9±0.8‡	9.6±0.8

All data were recorded at 1 Hz and shown as mean±SEM. APD90 indicates APD at 90%.

*$P<0.05$ versus control.

†$P<0.01$ versus control.

‡$P<0.001$ versus control.

Several recent studies have addressed the mechanisms of Ca^{2+} transient abnormalities associated with atrial pathology. Lenaerts et al[7] reported detailed studies in sheep with longstanding AF (average >4 months) and ventricular dysfunction. Like us, they observed striking APD abbreviations and reduced Ca^{2+} transients. I_{CaL} was diminished, but the reduction was limited when EGTA was omitted from the pipette. They also noted increased Na^+, Ca^{2+} exchange function and expression and emphasized the importance of reduced subsarcolemmal-RyR coupling efficiency along with loss of t-tubules. They did not examine the role of APD changes or

Downloaded from circep.ahajournals.org at Vrije on July 11, 2011

intrinsic contractile properties. Dibb et al[13] characterized Ca^{2+} release properties in sheep with ventricular tachypacing-induced heart failure. They noted substantial loss of t-tubules associated with impaired centripetal propagation of the Ca^{2+} signal from the subsarcolemma to the center of the cell. However, in rabbit atrial myocytes, ATR suppresses centripetal Ca^{2+} wave propagation despite a lack of t-tubules, pointing to mechanisms other than reduced t-tubular density.[12]

Several studies have suggested a prime role of atrial APD abbreviation in AF-related contractile dysfunction. Atrial contractility decreases rapidly in goats with electrically maintained AF, with a similar time-course to AERP abbreviation.[17] Administration of the K^+ channel blocker AVE0118 increases AERP and atrial contractility in contrast to absent or limited effects of other positive inotropic agents like digoxin, dobutamine, the Ca^{2+} sensitizer EMD57033, and the Ca^{2+} channel agonist BayY5959.[3] Similar effects of AVE0118 have been observed in RA trabeculae of patients with AF.[18] On the basis of this evidence, the use of APD-prolonging agents has been advocated to abrogate atrial hypocontractility in AF.[3]

MyBP-C dephosphorylation has been noted in atrial tissue samples from patients with AF.[6] No previous studies have noted changes in the expression and phosphorylation of MLC2a, an important regulator of cardiac contraction.[19] Eiras et al[20] described decreased force redevelopment in skinned muscle fibers from patients with dilated atria in both sinus rhythm and AF along with increased expression of β MHC protein, TnT, and desmin in patients with AF only. Most patients with AF had significant valvular heart disease (unlike the control, sinus rhythm, and dilated atria groups), which can markedly alter atrial function and gene expression.[21]

We noted changes in contractile protein (MyBP-C and MLC2a) phosphorylation that likely contributed to contractile abnormalities and addressed potential underlying mechanisms by studying changes in key phosphorylation (kinase) and dephosphorylation (phosphatase) systems. Consistent with previous data in patients with chronic AF and goats with sustained AF,[6,15] global PP1 activity was increased in ATR, whereas protein expression of the regulatory PKAIIα subunit (which coordinates targeting of the PKAc subunits to PKA targets) was reduced. Although we did not directly measure PP1 and PKA activities in the myofilament and SR compartments, greater local PP1, reduced PKA, or both activity likely underlies hypophosphorylation (and resulting dysfunction) of the 2 key cross-bridge cycling regulatory proteins MyBP-C and MLC2a at established PKA sites. PKA phosphorylation of RyR2 and PLB (Ser2809 and Ser16 sites, respectively) was preserved in ATR despite increased PP1 activity and reduced PKAIIα expression. In patients with chronic AF, SR-related PP1 function is reduced because of increased inhibitor 1 activity,[6] which controls PP1 activity exclusively at the SR, specifically targeting phosphorylation of PLB and RyR2 at Ser16 and Ser2815 sites, respectively.[22,23] Thus, reduced PP1 activity in the SR compartment of ATR dogs may offset reductions in PKAIIα expression at Ser16. On the other hand, although higher global activity of CaMKII in the face of reduced SR-related PP1 activity in ATR would be expected to increase phosphorylation at CaMKII phosphorylation sites of RyR2 and PLB (Ser2815 and Thr17, respectively), steady-state phosphorylation at these sites was unchanged. Further work clearly is needed to explain more fully SR PKA and CaMKII phosphorylation properties in ATR.

Novel Elements and Potential Significance

Atrial contractile remodeling has important clinical consequences, including increased atrial thrombogenesis and stroke risk in patients with AF.[24–26] Elucidating the underlying pathophysiological mechanisms may allow for the identification of new therapeutic targets. Whereas atrial contractility changes have been attributed previously to APD reduction based on indirect evidence,[3,15,17,18] our study is the first to our knowledge to examine directly the role of ATR-induced AP waveform alterations. By applying AP waveforms from control and ATR cardiomyocytes to cells from both types of dogs (Figure 4) we were able to conclude that ATR-induced AP changes do contribute significantly to Ca^{2+} release and contractile disturbances but that APD alterations account for only a minority of the abnormalities observed. We identified a range of additional contributors, indicating that the contractile dysfunction caused by ATR is multifactorial and implying that the targeting of any single pathophysiological component is unlikely to be successful. Indeed, despite the fact that the repolarization-prolonging agent AVE0118 was the most effective single intervention in restoring atrial contractility in AF remodeled goats,[3] atrial shortening velocity abnormalities were incompletely reversed (by 65% in RA and 75% in left atrium), whereas AERP was increased to 120% of pre-AF values.

ATR can cause APD abbreviation by several ionic mechanisms, including I_{CaL} reduction and increased inward rectifier currents.[21,27] The present study is the first to address the specific role of I_{CaL} reduction, independent of associated APD decreases, in ATR-induced Ca^{2+} release and contractile impairments. Our results indicate that I_{CaL} decreases produce disproportionate impairments by virtue of their combined effects on APD and Ca^{2+} entry through I_{CaL} channels.

Previous experimental studies of ATR AF-related contractile dysfunction have used animals with uncontrolled ventricular responses,[2,3,7,15] resulting in varying degrees of ventricular dysfunction known to importantly alter atrial cardiomyocyte subcellular properties and Ca^{2+} handling.[13] Here, we show that relatively short-term (7-day) ATR itself, with a controlled ventricular response and unaltered ventricular function (Table 2), significantly depresses atrial contractility through a variety of cellular and subcellular mechanisms.

Potential Limitations

We chose a 1-week period of ATR based on the fact that ion current changes caused by ATR reach near steady-state after 1 week.[4] Shapiro et al[28] showed that patients with acute AF (mean duration, 1.8 days) do not show significant postcardioversion atrial dysfunction, whereas AF lasting longer than 1 week causes substantial atrial contractile abnormalities that require several days to recover. ATR lasting for considerably

Downloaded from circep.ahajournals.org at Vrije on July 11, 2011

longer periods could produce further changes in contractility involving additional mechanisms where the existence of slowly developing components to AF remodeling is well recognized.[29,30] Nevertheless, the contractility changes that we observed are quite similar to those noted by Lenaerts et al[7] after a mean 129-day AF period in sheep.

Our studies indicate that a variety of mechanisms likely contribute to ATR-induced Ca^{2+} release and contractile abnormalities, which is somewhat unsatisfying because the precise contribution of each individual component is difficult to assess and may vary with the duration of ATR, presence of associated heart disease, drug therapy, and so forth. As unappealing as this biological reality is, it is important to appreciate that the variety of mechanisms contributing to atrial contractile dysfunction after as few as 7 days of ATR suggests that therapies targeting common upstream signaling events or rapid atrial activation itself may be more effective than attempting to intervene at the level of specific downstream pathophysiological contributors to hypocontractility.

Acknowledgments

We thank Nathalie L'Heureux, Chantal St-Cyr, Audrey Bernard, Manja Schöne, Annett Opitz, and Sabine Kirsch for technical support and France Thériault for secretarial help with the manuscript.

Sources of Funding

This study was supported by the Canadian Institutes of Health Research (MOP 44365), the Quebec Heart and Stroke Foundation, St Jude Medical Scholarship of the German Cardiac Society (to Dr Wakili), the German Federal Ministry of Education and Research (Atrial Fibrillation Competence Network grant 01Gi0204), a network grant from Fondation Leducq (ENAFRA Network, 07/CVD/03), the MITACS Network, Chang Gung Memorial Hospital award CMRPG370141-3, and German Research Foundation grant DFG-BO-1263/9-1.

Disclosures

Dr. Nattel is listed as inventor on a patent owned by the Montreal Heart Institute and Université de Montréal, entitled "Statin drugs to treat atrial fibrillation."

References

1. Wolf PA, Abbott RD, Kannel WB. Atrial fibrillation as an independent risk factor for stroke: the Framingham Study. *Stroke*. 1991;22:983–988.
2. Sun H, Gaspo R, Leblanc N, Nattel S. Cellular mechanisms of atrial contractile dysfunction caused by sustained atrial tachycardia. *Circulation*. 1998; 98:719–727.
3. de Haan S, Greiser M, Harks E, Blaauw Y, van Hunnik A, Verheule S, Allessie M, Schotten U. AVE0118, blocker of the transient outward current (I_{to}) and ultrarapid delayed rectifier current (I_{Kur}), fully restores atrial contractility after cardioversion of atrial fibrillation in the goat. *Circulation*. 2006;114:1234–1242.
4. Yue L, Feng J, Gaspo R, Li GR, Wang Z, Nattel S. Ionic remodeling underlying action potential changes in a canine model of atrial fibrillation. *Circ Res*. 1997;81:512–525.
5. Schotten U, Ausma J, Stellbrink C, Sabatschus I, Vogel M, Frechen D, Schoendube F, Hanrath P, Allessie MA. Cellular mechanisms of depressed atrial contractility in patients with chronic atrial fibrillation. *Circulation*. 2001;103:691–698.
6. El-Armouche A, Boknik P, Eschenhagen T, Carrier L, Knaut M, Ravens U, Dobrev D. Molecular determinants of altered Ca^{2+} handling in human chronic atrial fibrillation. *Circulation*. 2006;114:670–680.
7. Lenaerts I, Bito V, Heinzel FR, Driesen RB, Holemans P, D'hooge J, Heidbüchel H, Sipido KR, Willems R. Ultrastructural and functional remodeling of the coupling between Ca^{2+} influx and sarcoplasmic reticulum Ca^{2+} release in right atrial myocytes from experimental persistent atrial fibrillation. *Circ Res*. 2009;105:876–885.
8. Khan IA. Atrial stunning: basics and clinical considerations. *Int J Cardiol*. 2003;92:113–128.
9. Bers DM. Cardiac excitation-contraction coupling. *Nature*. 2002;415: 198–205.
10. Van Wagoner DR, Pond AL, Lamorgese M, Rossie SS, McCarthy PM, Nerbonne JM. Atrial L-type Ca^{2+} currents and human atrial fibrillation. *Circ Res*. 1999;85:428–436.
11. Bosch RF, Scherer CR, Rüb N, Wöhrl S, Steinmeyer K, Haase H, Busch AE, Seipel L, Kühlkamp V. Molecular mechanisms of early electrical remodeling: transcriptional downregulation of ion channel subunits reduces $I_{Ca,L}$ and I_{to} in rapid atrial pacing in rabbits. *J Am Coll Cardiol*. 2003;41:858–869.
12. Greiser M, Verheule S, Allessie MA, Schotten U. Functional but not structural changes underlie failure of intracellular Ca^{2+} wave propagation in tachycardia-induced remodeling [abstract]. *Circulation*. 2008; 118:S438.
13. Dibb KM, Clarke JD, Horn MA, Richards MA, Graham HK, Eisner DA, Trafford AW. Characterization of an extensive transverse tubular network in sheep atrial myocytes and its depletion in heart failure. *Circ Heart Fail*. 2009;2:482–489.
14. Grimm M, Mahnecke N, Soja F, El-Armouche A, Haas P, Treede H, Reichenspurner H, Eschenhagen T. The MLCK-mediated alpha1-adrenergic inotropic effect in atrial myocardium is negatively modulated by PKCepsilon signaling. *Br J Pharmacol*. 2006;148:991–1000.
15. Greiser M, Neuberger HR, Harks E, de Haan S, Verheyen F, Boknik P, El-Armouche A, Schmitz W, Ravens U, Nattel S, Allessie MA, Dobrev D, Schotten U. Distinct contractile and molecular difference between two goat models of atrial dysfunction: AV-block-induced atrial dilatation and atrial fibrillation. *J Mol Cell Cardiol*. 2009;46:385–394.
16. Logan WFWE, Rowlands DJ, Howitt G, Holmes AM. Left atrial activity following cardioversion. *Lancet*. 1965;2:471–473.
17. Schotten U, Duytschaever M, Ausma J, Eijsbouts S, Neuberger HR, Allessie M. Electrical and contractile remodeling during the first days of atrial fibrillation go hand in hand. *Circulation*. 2003;107:1433–1439.
18. Schotten U, de Haan S, Verheule S, Harks EG, Frechen D, Bodewig E, Greiser M, Ram R, Maessen J, Kelm M, Allessie M, Van Wagoner DR. Blockade of atrial-specific K^+-currents increases atrial but not ventricular contractility by enhancing reverse mode Na^+/Ca^{2+}-exchange. *Cardiovasc Res*. 2007;73:37–47.
19. Chan JY, Takeda M, Briggs LE, Graham ML, Lu JT, Horikoshi N, Weinberg EO, Aoki H, Sato N, Chien KR, Kasahara H. Identification of cardiac-specific myosin light chain kinase. *Circ Res*. 2008;102:571–580.
20. Eiras S, Narolska NA, van Loon RB, Boontje NM, Zaremba R, Jimenez CR, Visser FC, Stooker W, van der Velden J, Stienen GJ. Alterations in contractile protein composition and function in human atrial dilatation and atrial fibrillation. *J Mol Cell Cardiol*. 2006;41:467–477.
21. Gaborit N, Steenman M, Lamirault G, Le Meur N, Le Bouter S, Lande G, Léger J, Charpentier F, Christ T, Dobrev D, Escande D, Nattel S, Demolombe S. Human atrial ion channel and transporter subunit gene-expression remodeling associated with valvular heart disease and atrial fibrillation. *Circulation*. 2005;112:471–481.
22. El-Armouche A, Wittköpper K, Degenhardt F, Weinberger F, Didie M, Grimm M, Melnychenko I, Peeck M, Zimmermann WH, Unsöld B, Hasenfuss G, Dobrev D, Eschenhagen T. Phosphatase inhibitor-1-deficient mice are protected from catecholamine-induced arrhythmias and myocardial hypertrophy. *Cardiovasc Res*. 2008;80:396–406.
23. Wittköpper K, Fabritz L, Neef S, Ort K, Grefe C, Unsöld B, Kirchhof P, Maier LS, Hasenfuß G, Dobrev D, Eschenhagen T, El-Armouche A. Conditional overexpression of constitutively active phosphatase-1-inhibitor-1 improves cardiac contractility in young mice but is deleterious after catecholaminergic stress and with aging. *J Clin Invest*. 2010;120: 617–626.
24. Fatkin D, Kuchar DL, Thorburn CW, Feneley MP. Transesophageal echocardiography before and during direct current cardioversion of atrial fibrillation: evidence for "atrial stunning" as a mechanism of thromboembolic complications. *J Am Coll Cardiol*. 1994;23:307–316.
25. Missault L, Jordaens L, Gheeraert P, Adang L, Clement D. Embolic stroke after unanticoagulated cardioversion despite prior exclusion of atrial thrombi by transoesophageal echocardiography. *Eur Heart J*. 1994; 15:1279–1280.

Downloaded from circep.ahajournals.org at Vrije on July 11, 2011

26. Dunn MI, Marcum JL. Atrial mechanical performance following internal and external cardioversion of atrial fibrillation: its relationship to peripheral embolization and acute cerebrovascular accident. *Chest*. 2002;121:1–3.
27. Nattel S, Maguy A, Le Bouter S, Yeh YH. Arrhythmogenic ion-channel remodeling in the heart: heart failure, myocardial infarction, and atrial fibrillation. *Physiol Rev*. 2007;87:425–456.
28. Shapiro EP, Effron MB, Lima S, Ouyang P, Siu CO, Bush D. Transient atrial dysfunction after conversion of chronic atrial fibrillation to sinus rhythm. *Am J Cardiol*. 1988;62:1202–1207.
29. Ausma J, Litjens N, Lenders MH, Duimel H, Mast F, Wouters L, Ramaekers F, Allessie M, Borgers M. Time course of atrial fibrillation-induced cellular structural remodeling in atria of the goat. *J Mol Cell Cardiol*. 2001;33:2083–2094.
30. Todd DM, Fynn SP, Walden AP, Hobbs WJ, Arya S, Garratt CJ. Repetitive 4-week periods of atrial electrical remodeling promote stability of atrial fibrillation: time course of a second factor involved in the self-perpetuation of atrial fibrillation. *Circulation*. 2004;109:1434–1439.

CLINICAL PERSPECTIVE

Atrial fibrillation diminishes atrial contractility, even after sinus rhythm is restored, potentially contributing to thrombogenicity. In a canine model, we found that 1 week of 400-bpm atrial tachycardia decreases atrial contractility and action potential duration. In contrast to prior suggestions, we found that shortening of action potential duration alone is not sufficient to explain the decrease in contractility. Tachycardia-induced reductions in L-type calcium current independently reduce calcium transients and cell contraction. Modifications in subcellular calcium handling that impair transmission of calcium release signals from the cell surface to the contractile apparatus were present. Furthermore, changes in contractile protein regulation by phosphorylation may impair contractile element function. Thus, rapid atrial tachycardia, as occurs in atrial fibrillation, impairs atrial contractile function by multiple mechanisms, including, but not limited to, action potential duration abbreviation. These findings suggest that atrial contractility may be more effectively improved by approaches directed at common upstream mechanisms rather than modulating action potential duration alone.

Downloaded from circep.ahajournals.org at Vrije on July 11, 2011

Supplemental Material

Detailed Materials and Methods

Animal Model

Sixty-three adult mongrel dogs (22-36 kg) were divided into two groups: 1) control (CTL, n=35) and 2) 1-week atrial tachycardia remodeling (ATR, n=28). ATR dogs were initially anesthetized with diazepam (0.25 mg/kg IV)/ketamine (5.0 mg/kg IV)/halothane (1% to 2%). Unipolar leads were inserted fluoroscopically into the right-ventricular apex (RV) and right-atrial (RA) appendage, and connected to separate pacemakers implanted in the neck. Atrioventricular (AV) block was created by radiofrequency-ablation to control ventricular rate during ATR. The RV-pacemaker was programmed to 80 bpm. After 24-hour recovery, the atrial pacemaker was programmed to pace the RA at 400 bpm for 7 days.

On study days the atrial pacemaker was deactivated and an open-chest electrophysiological study was performed. Dogs were anaesthetized with morphine (2 mg/kg SC) and α-chloralose (120 mg/kg IV, followed by 29.25 mg/kg per hour) and ventilated mechanically. RA-appendage effective refractory periods (ERPs) were determined at basic cycle lengths (BCLs) of 150, 200, 250, 300 and 360 ms with 8 basic stimuli followed by one premature stimulus (5-ms decrements). AF (an irregular atrial rhythm>400 bpm) was induced by burst pacing. Mean AF duration was determined in each dog as an index of the AF-maintaining substrate in that dog. Mean±SEM AF-duration was calculated in each experimental group as previously described, based on the average individual AF-duration values in each dog. Hemodynamic data were measured with fluid-filled catheters and transducers. All animal-care and -handling procedures were in accordance to National Institutes of Health guidelines, and were reviewed and approved by the Animals Research Ethics Committee of The Montreal Heart Institute.

Downloaded from circep.ahajournals.org at Vrije on July 11, 2011

Transthoracic Echocardiography

Transthoracic echocardiography was performed under sedation (Atravet 0.07 mg/kg and buprenorphine 0.009 mg/kg IM) with an M3S probe (2.0-4.3 Megaherz) and a Vivid 7 Dimension system (GE Healthcare Ultrasound, Horten, Norway). All recordings were performed in sinus rhythm, with atrial tachypacemakers turned off to permit accurate analyses under comparable conditions. To study left-atrial (LA) emptying and contractile function, an apical 4-chamber view was obtained, LA area in both cardiac systole (defined as the largest) and cardiac diastole (defined as the smallest) was measured. M-mode echocardiogram was obtained at the aortic-valve level in the parasternal long axis view to measure LA-diameters. Atrial fractional shortening was calculated as (systolic area-diastolic area)/systolic area×100% for area; and (systolic diameter-diastolic diameter)/systolic diameter×100% for diameter. Pulsed-wave Doppler was used to study transmitral flow in the apical 4-chamber view. Peak velocity in early filling e-wave, and atrial filling a-wave (following a sinus p wave between two QRS deflections on a simultaneously-recorded ECG) were obtained, and e/a-ratio was calculated. The average of three to six cardiac cycles was used for each and all measurements, with the operator blinded to treatment assignment.

Cardiomyocyte Isolation and Frozen-Tissue Samples

After open-chest studies, hearts and adjacent lung tissues were excised through a median thoracotomy and immersed in oxygenated Tyrode solution at room temperature. RA-tissue from n=10 ATR and n=14 control dogs was dissected and immediately frozen in liquid nitrogen for molecular biology experiments. For cellular studies, RA preparations were dissected from n=21 control and n=18 ATR dogs and afterwards coronary-perfused at ~10 mL/min for cardiomyocyte

Downloaded from circep.ahajournals.org at Vrije on July 11, 2011

isolation as previously-described (Qi et al, 2008). Perfusion was performed with Ca^{2+}-free Tyrode solution containing collagenase (110 U/mL CLS II collagenase; Worthington Biochemical, Lakewood, NJ) and 0.1% bovine serum albumin for ~40 min, following which single cells were obtained by trituration.

Cellular shortening

Isolated cardiomyocytes were field-stimulated via 10-ms 1.5×threshold square-wave pulses at a temperature of 35°C. Cell-shortening was measured with a video edge-detector, with edge-detection cursors positioned at both cell-ends to measure whole-cell shortening. Cell-shortening data was calculated based on the average of 10 consecutive beats. Additionally, we analyzed cell-length changes as a function of time by calculating the maximum contracting ($+\Delta L/\Delta t$) and relaxing ($-\Delta L/\Delta t$) slopes of the cell-shortening curve.

In AP-clamp experiments, attachment of the patch pipette to the center of atrial cells often affected motion of the cell center, which very often resulted in non-linear contraction of one cell edge with preserved motion of the other edge. Because of this phenomenon, cellular shortening measurements in AP-clamp experiments were always based on absolute shortening of the normally-moving cell edge (in µm).

Ca^{2+}-fluorescence Measurements

$[Ca^{2+}]_i$-transients were recorded with microfluorimetry. Fluorescence measurements were performed with Indo-1AM. After an incubation period of 4 min with 5-µmol/l Indo-1 AM, cells were superfused at 35°C with Tyrode solution (1.8 mmol/L Ca^{2+}) for 20 min. Cells were excited with ultraviolet light (340 nm), while emission was detected at 400 nm and 500 nm with two

Downloaded from circep.ahajournals.org at Vrije on July 11, 2011

separate photomultiplier tubes through a 10-μm aperture focused on the cardiomyocyte. Emission ratios (400 nm/500 nm, $R_{400/500}$) were calculated and used to determine $[Ca^{2+}{}_i]$.

Ratiometric $Ca^{2+}{}_i$-measurements were converted into intracellular Ca^{2+}-concentration ($[Ca^{2+}]_i$) according to Grynkiewicz et al with the formula $[Ca^{2+}]_i = Kd \times \beta \times (R_{400/500}\text{-}Rmin)/(Rmax\text{-}R_{400/500})$ as previously described (Qi et al, 2009). Sarcoplasmic reticulum (SR) Ca^{2+}-content was assessed based on the response to 10-second 10-mmol/L caffeine application *via* a rapid-perfusion system. The decay time-constant (τ) was calculated based on a monoexponential fit to the $[Ca^{2+}]_i$-decay curve.

Isolated cardiomyocytes from additional control and ATR-dogs were also studied by confocal microscopy to analyze subcellular Ca^{2+}-transient properties. Atrial cardiomyocytes were incubated with the Ca^{2+}-indicator Fluo-4-AM and placed in a perfusion chamber. Confocal microscopy was performed with an inverted microscope (Olympus IX 81, Olympus Canada, Markham, Ontario) equipped with a confocal laser line-scanning unit (Olympus Fluoview FV 1000). Ca^{2+}-transients were recorded under steady state field stimulation at 1 Hz. Line-scanning was performed with an optical resolution of 512×512 pixels and a temporal resolution of 1.8-2.0 ms/line. For longitudinal cell-scanning the lines were placed in the middle of the cell in a longitudinal direction; for transverse scans, lines were positioned at a 90° angle to the longitudinal cell axis, avoiding the nucleus. In addition z-scans were performed to confirm a central position in the z-axis. Analysis was performed with Fluoview analysis software (FV10-ASW 2.0, Olympus Canada). For longitudinal scans, three regions of interest (width 10 μm) were placed over the left lateral, right lateral, and over the central part of the cell (see Online-Figure 8A and C) to determine subcellular Ca^{2+}-transients. For transverse scans, 2 regions of interest (width 2 μm) were placed over the subsarcolemmal (SSL) and central part of the cell (see

Downloaded from circep.ahajournals.org at Vrije on July 11, 2011

Figure 5A and B). For mean-data analysis, 5 consecutive beats of each region of interest were averaged per cell and afterwards per dog, allowing a comparison of lateral (longitudinal scans) or subsarcolemmal (transverse scans) to central Ca^{2+}-transient amplitudes. Fluorescence intensity values (F) were normalized to the minimal end-diastolic fluorescence intensity (F_0) in each region of interest, resulting in F/F_0 ratios. Ca^{2+}-transient values are represented as $\Delta F/F_0$ indicating $(F_{max}- F_0)/ F_0$.

T-tubule network analysis:

Freshly isolated atrial cells from CTL dogs (n=3) and ATR dogs (n=3) were plated on laminin (Sigma) coated glass-bottomed Petri dishes (Fluorodishes, World Precision Instruments, Sarasota, FL). Cells were labeled with 2 μmol/L of the membrane marker di-4-ANEPPS (Invitrogen, Burlington, ON) diluted in Tyrode solution. Image acquisition started 2 minutes post-staining and never lasted more than 15 minutes to prevent di-4-ANEPPS intracellular accumulation. Samples were excited with an argon (488-nm) laser and emitted fluorescence over 515-nm Z-series (250 nm) was acquired with an LSM 710 confocal microscope (Carl Zeiss, Toronto, ON) using an LD LCI Plan-Apochromat 25×/0.8 Imm. Korr DIC set for water immersion. The calculated point spread function (cPSF) of the imaging system was obtained using 170-nm diameter fluorescent latex beads (Invitrogen) imaged at an x-y resolution of 41 nm and vertical z stacks of 250 nm separation. Experiments were carried out at 37ºC. Acquired z-series were deconvolved using maximum likelihood estimation with a Richardson-Lucy algorithm following Gaussian pre-filtering implemented with Huygens Professional 3.5.0; Scientific Volume Imaging, Hilversum, Netherlands (van Kempen et al, 1996). The z-sections were further iso-sampled (Huygens Pro, SVI) in order to make the z-spacing the same as the x-y. In each case, the distance to the surface

Downloaded from circep.ahajournals.org at Vrije on July 11, 2011

sarcolemmal membrane was determined to crop 2-µm thickness z-central sections avoiding the top and bottom surfaces. Any fluorescent objects outside the cell were removed by editing images with Zen software (Carl Zeiss). Cropped sections were rendered as Maximum Intensity Projections. Resulting projections were analyzed by excluding the cell membrane and quantifying intracellular membrane staining. The inner face of cardiomyocyte sarcolemmal membranes was used to determine the contour of the intracellular space within the projections. The surface of the resulting intracellular region was then determined and the mean pixel intensity calculated. T-tubule density was estimated from the mean pixel intensity normalized to the surface area of the intracellular region for each cardiomyocyte.

Cellular Electrophysiology

Action-potential (AP) recordings were performed with whole-cell perforated-patch technique and current-clamp mode. Tip resistances were between 3 and 5 MΩ. Pipette tips were filled with nystatin-free intracellular solution by capillary action, and pipettes were then back-filled with nystatin-containing (600-µg/ml) pipette solution. Average junction potentials were 15.9 mV and were corrected for AP-recordings only. All recordings were performed at 35±0.5°C.

Normal Tyrode solution contained (mmol/L): NaCl 136, KCl 5.4, $MgCl_2$ 1, $CaCl_2$ 1.8, NaH_2PO_4 0.33, HEPES 5 and dextrose 10 (pH 7.4, NaOH). The pipette solution for AP-recording contained (mmol/L) GTP 0.1, K^+-aspartate 110, KCl 20, $MgCl_2$ 1, ATP-Mg 5, HEPES 10, Na_2-phosphocreatine 5, and EGTA 0.05, pH 7.4 (KOH).

For L-Type Ca^{2+} current ($I_{Ca,L}$) measurement the extracellular solution contained (in mmol/L) tetraethylammonium chloride 136, CsCl 5.4, $MgCl_2$ 1, $CaCl_2$ 2, NaH_2PO_4 0.33, dextrose 10, and HEPES 5, titrated to pH 7.4 with CsOH. Niflumic acid (50-µmol/L) was added to inhibit Ca^{2+}-dependent Cl^--current, and 4-aminopyridine (2-mmol/L) was added to suppress I_{to}. The

Downloaded from circep.ahajournals.org at Vrije on July 11, 2011

pipette solution for $I_{Ca,L}$-recording contained (mmol/L) CsCl 120, tetraethylammonium chloride 20, $MgCl_2$ 1, EGTA 10, MgATP 5, HEPES 10, and Li-GTP 0.1, titrated to pH 7.4 with CsOH. For separate experiments evaluating the contribution of Ca^{2+}-dependent $I_{Ca,L}$ inactivation to $I_{Ca,L}$ measurements in control and ATR cells, EGTA was withdrawn from the pipette solution to exclude EGTA-related Ca^{2+} buffering effects.

AP voltage-clamp (whole-cell perforated patch) was used to evaluate AP-dependent effects on Ca^{2+} transients and cell shortening. RA-cardiomyocytes were subjected to typical AP-waveforms from control and ATR cardiomyocytes at 2 Hz for sequential 6-min periods (in randomized order). Parallel Ca^{2+} transients (10-20 beats) were recorded in 120-s intervals. For analysis all Ca^{2+}-transients obtained during the 6-min periods were averaged and mean±SEM were calculated within each AP-waveform group.

Force Measurements in Single Skinned Cardiomyocytes

Cardiomyocytes were mechanically isolated, permeabilized and mounted in the experimental set-up as described previously (Van der Velden et al, 2003). Isometric force measurements were performed at 15°C and a resting sarcomere length of 2.2 μm. The rate of force redevelopment was determined during activation at different Ca^{2+}-concentrations when the steady isometric force level was reached, by rapidly (<1 ms) shortening the myocyte by 20% and, after a delay of 30 ms, restretching it to the original length (L_o). Force redevelopment after the restretch was fitted to a single exponential (Marquart-Levenberg algorithm, Kaleidograph, Synergy Software, Reading, PA) to estimate the rate of force redevelopment (K_{TR}). Passive force ($F_{passive}$) was determined in relaxing solution by applying the same shortening (20% of L_o) followed by a restretch after 10 s.

Downloaded from circep.ahajournals.org at Vrije on July 11, 2011

Western Blot and Phosphatase-activity Measurements

RA-tissue homogenates were prepared from freeze-dried tissue and protein concentrations determined with Amido-Black 10B. Protein-expression was quantified as previously described (El-Armouche et al, 2006). Proteins were fractionated on SDS-polyacrylamide gels and transferred to nitrocellulose membranes (BioTrace®NT, Life Sciences, Pall Corporation, Port Washington, NY). Western blotting was performed with primary antibodies to GAPDH (1:100000; HyTest, Turku, Finland), calsequestrin (1:2500; Dianova, Hamburg, Germany), troponin-I (Tn-I, 1:30000; Chemicon, Millipore, Billerica, MA), Ser23/24 phosphorylated Tn-I (1:5000; Cell Signaling, City, State), troponin-C (monoclonal; 1:1000; Fitzgerald, North Acton, MA), phosphorylated myosin-light-chain-2a (MLC2a, 1:10000; kind gift from Dr Thomas Eschenhagen, University of Hamburg, Hamburg, Germany), SR Ca^{2+}-ATPase (SERCA2a, 1:2000; Santa Cruz, Santa Cruz, CA), Thr-287 phosphorylated Ca^{2+}-calmodulin protein kinase-II (CaMKII) (1:5000; Promega, Madison, WI), CaMKIIδ (1:200; Santa Cruz), catalytic protein-kinase A (PKA)-subunit (1:1000, BD Transduction Laboratories, Mississauga, Canada), regulatory PKA IIα-subunit (1:500, Santa Cruz), total phospholamban, Ser-16 and Thr-17 phosphorylated phospholamban (all 1:5000; Badrilla, Leeds, UK), protein phosphatase 1α (PP1α, 1:500; Biomol, Hamburg, Germany), protein phosphatase 2A (PP2A, 1:2000, affinity purified; Upstate Biotechnology, Millipore), Na^{+}/Ca^{2+}-exchanger (NCX1, 1:1000; Affinity BioReagents, Thermo Scientific, Waltham, MA), total myosin-binding protein C (MyBP-C, 1:5000), and Ser-282 phosphorylated MyBP-C (1:1000; kind gifts from Dr Lucie Carrier, University of Hamburg, Hamburg, Germany), total ryanodine receptor (RyR2), and Ser-2809 and Ser-2815 phosphorylated RyR2 (1:5000, 1:5000 and 1:2500, respectively; kind gifts from Dr Andrew Marks, Columbia University, New York, NY). Detection was performed with suitable secondary

Downloaded from circep.ahajournals.org at Vrije on July 11, 2011

antibodies and protein bands were visualized with electrochemoluminescence reagents (Thermo Scientific) and Hyperfilm-ECL (GE Healthcare, Little Chalfont, UK). The films were evaluated densitometrically with Phoretix 1D software (Biostep, Jahnsdorf, Germany). Atrial homogenates were used to measure phosphatase-activity. Serine/threonine protein-phosphatase activity was assessed with phosphorylase-A as substrate, and quantified as nanomoles of ^{32}Pi released per milligram protein/minute. Differentiation between PP1 and PP2A activities measurements was obtained with okadaic acid (3 nmol/L).

Myosin heavy chain and titin isoforms

The myosin heavy chain isoform (MHC) composition was analyzed by one-dimensional SDS polyacrylamide gel electrophoresis (SDS-PAGE) according to previously-described methods (Neagoe et al, 2002; Warren et al, 2003). The separating gel contained 12% total acrylamide (acrylamide to bis-acrylamide ratio 200:1; pH 9.3), while the stacking gel contained 3.5% total acrylamide (acrylamide to bis-acrylamide ratio 20:1; pH 6.8). Gels were silver-stained and analyzed by laser densitometry. To check for linearity, different amounts of protein were loaded on the gels and the density of the MHC bands was determined. Only samples within the linear range (typically 0.2-1.0 μg of total protein) were used in the evaluation.

Dog atria were homogenized in modified Laemmli buffer and agarose-strengthened 2% SDS-PAGE to detect titin was performed as described (Neagoe et al, 2002; Opitz et al, 2004). Protein-bands were visualized with Imperial protein stain, scanned, and analyzed densitometrically. Average titin isoform composition was calculated from 10 measurements per experimental condition.

Downloaded from circep.ahajournals.org at Vrije on July 11, 2011

Data Analysis

The force-pCa relation was fit by a non-linear procedure to the Hill equation: $F(Ca^{2+})/F_{max} = [Ca^{2+}]^{nH}/(Ca_{50}{}^{nH}+[Ca^{2+}]^{nH})$, where F is steady-state force at different Ca^{2+} concentrations. F_{max} denotes the active steady isometric force component developed at saturating Ca^{2+}-concentration. The Hill coefficient (nH) is a measure of the steepness of the relationship, and Ca_{50} (or pCa_{50}) represents the Ca^{2+} concentration at which tension= $0.5\times F_{max}$, i.e. the mid-point of the relation.

All data are presented as mean±SEM. For single comparisons paired or non-paired t-tests were applied as appropriate. Repeated-measures analyses were performed with two-way ANOVA. When significant interactions were found between main-effects, Bonferroni-corrected *t*-tests were applied to determine the levels of the repeated measure at which significant differences occurred (the P-values shown were obtained by multiplying each P by the number of repeated tests performed). In the absence of interaction, the significance of main-effect differences is shown. Analyses of non-repeated measurements in multiple groups (control versus 24-hour recovery versus 48-hour recovery) were performed by one-way ANOVA, followed (if significant) by least-significant difference test. The specific statistical test applied for each analysis follows:

- Figures 1C, D, E: non-paired t-tests.
- Figures 2B, C : non-paired t-tests.
- Figure 2E : 2-way ANOVA for repeated measures; main effect factors: group (CTL vs ATR), frequency; significant group effect for CTL vs ATR; no significant interaction.
- Figures 3 B, C: non-paired t-tests.

Downloaded from circep.ahajournals.org at Vrije on July 11, 2011

- Figure 3E: 2-way ANOVA for repeated measures; main effect factors: group (CTL vs ATR), frequency; significant group effect for CTL vs ATR; no significant interaction.
- Figure 3F: 2-way ANOVA; main effect factors: group (CTL vs ATR), test potential (TP); significant interaction between TP and group, individual P-values at each TP by Bonferroni-corrected t-test (corrected values are shown).
- Figures 4B, C, E, F: paired t-tests (each set of observations was based on repeated measures under each condition in each cell).
- Figure 5B: 1-way ANOVA, individual P-values by least significant difference test.
- Figure 6: non-paired t-tests.
- Figure 7: non-paired t-tests.
- Figure 8: non-paired t-tests.

- Tables 1 and 2: non-paired t-tests.
- Table 3: 1-way ANOVA, individual P-values by least significant difference test.

- On-line Figure I : 2-way ANOVA for repeated measures; main effect factors: group (CTL vs ATR), frequency; significant group effect for CTL vs ATR; no significant interaction.
- On-line Figure II : 2-way ANOVA for repeated measures; main effect factors group (CTL vs ATR), frequency; no significant group effects or interaction.
- On-line Figure III : 2-way ANOVA for repeated measures; main effect factors group (CTL vs ATR), test potential (panels A-C), P1-P2 interval (D); no significant group effects or interaction.
- On-line Fig IVB : 2-way ANOVA for repeated measures; main effect factors group (CTL

Downloaded from circep.ahajournals.org at Vrije on July 11, 2011

vs ATR), test potential; significant interaction between group and test potential; individual P-values at different test potentials by Bonferroni-corrected t-test (corrected values are shown).

- On-line Figures VA and B: 2-way ANOVA for repeated measures; main effect factors group (CTL vs ATR), test potential; panel A: no significant interaction, significant main effect for group is shown. No significant interaction or main effect in panel B.
- On-line Figure VC: Non-paired t-tests for group (control vs ATR) activation and inactivation V1/2 values shown in insets.
- On-line Figure VD: non-paired t-test on time constants shown in inset.
- On-line Figure VI: non-paired t-tests.
- On-line Figure VII : 2-way ANOVA for repeated measures; main effect factors group (CTL vs ATR), frequency; significant group effect for group (CTL vs ATR); no significant interaction.
- On-line Figure VIII: non-paired t-tests.
- On-line Figure IX: illustrates raw data from one sample from each group, results for mean data mentioned in text are compared by non-paired t-test.
- On-line Figure X: non-paired t-tests.
- On-line Figure XIA : 2-way ANOVA for repeated measures; main effect factors group (CTL vs ATR), frequency; significant group effect for group (CTL vs ATR); no significant interaction.
- On-line Figures XIB, XIC: 1-way ANOVA with least significant difference test.

A 2-tailed $P<0.05$ was considered statistically-significant. The authors had full access to

Downloaded from circep.ahajournals.org at Vrije on July 11, 2011

the data and take responsibility for its integrity. All authors have read and agree to the manuscript as written.

Downloaded from circep.ahajournals.org at Vrije on July 11, 2011

Online-References:

El-Armouche A, Boknik P, Eschenhagen T, Carrier L, Knaut M, Ravens U, Dobrev D. Molecular determinants of altered Ca^{2+} handling in human chronic atrial fibrillation. *Circulation*. 2006;114:670-680.

Neagoe C, Kulke M, del Monte F, Gwathmey JK, de Tombe PP, Hajjar RJ, Linke WA. Titin isoform switch in ischemic human heart disease. *Circulation.* 2002;106:1333-1341.

Opitz CA, Leake MC, Makarenko I, Benes V, Linke WA. Developmentally regulated switching of titin size alters myofibrillar stiffness in the perinatal heart. *Circ Res.* 2004;94:967-975.

Popov N, Schmitt M, Schulzeck S, Matthies N. Reliable micromethod for determination of the protein content in tissue homogenates. *Acta Biol Med Ger*. 1975;34:1441-1446.

Qi XY, Yeh YH, Xiao L, Burstein B, Maguy A, Chartier D, Villeneuve LR, Brundel BJ, Dobrev D, Nattel S. Cellular signaling underlying atrial tachycardia remodeling of L-type calcium current. *Circ Res.* 2008;103:845-854.

Qi X, Yeh YH, Chartier D, Xiao L, Tsuji Y, Brundel BJ, Kodama I, Nattel S. The calcium/calmodulin/kinase system and arrhythmogenic afterdepolarizations in bradycardia-related acquired long-QT syndrome. *Circ Arrhythm Electrophysiol.* 2009;2:295-304.

van der Velden J, Papp Z, Boontje NM, Zaremba R, de Jong JW, Janssen PM, Hasenfuss G, Stienen GJM. The effect of myosin light chain 2 dephosphorylation on Ca^{2+}-sensitivity of force is enhanced in failing human hearts. *Cardiovasc Res*. 2003;57:505-514.

Van Kempen GMP, van Vliet LJ, Verveer PJ, van der Voort HTM. A quantitative comparison of image restoration methods for confocal microscopy. *J Microscopy*. 1996;185:354-365.

Warren CM, Krzesinski PR, Greaser ML. Vertical agarose gel electrophoresis and electroblotting of high-molecular-weight proteins. *Electrophoresis.* 2003;24:1695-1702.

Downloaded from circep.ahajournals.org at Vrije on July 11, 2011

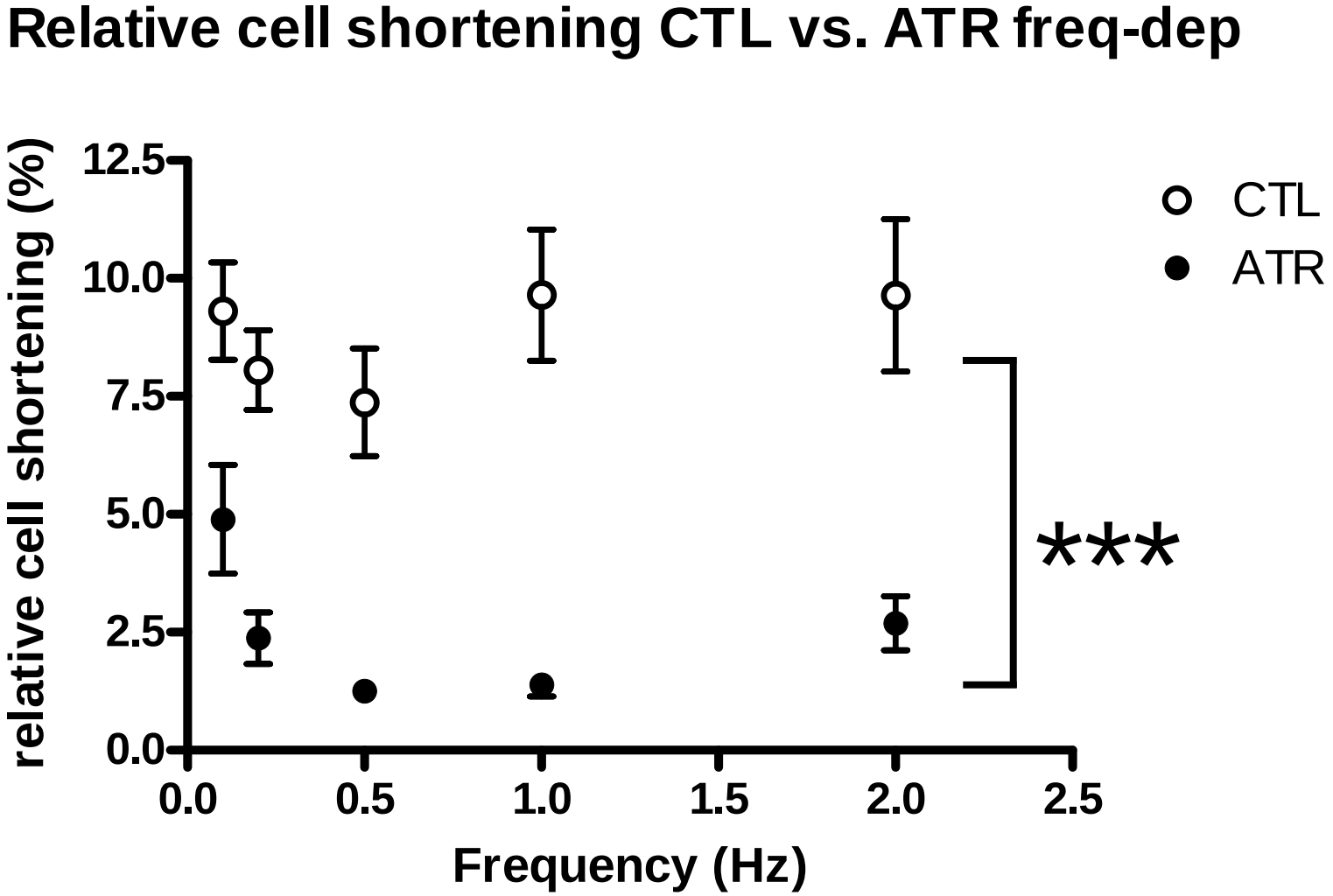

Online Figure 1. Relative cell shortening control (CTL) vs. ATR frequency dependence. Mean±SEM relative cell shortening as function of stimulation frequency (n=11 cells for CTL, n=14 cells for ATR, ****P*<0.001 ATR vs. CTL, effect of group).

Online Figure 2

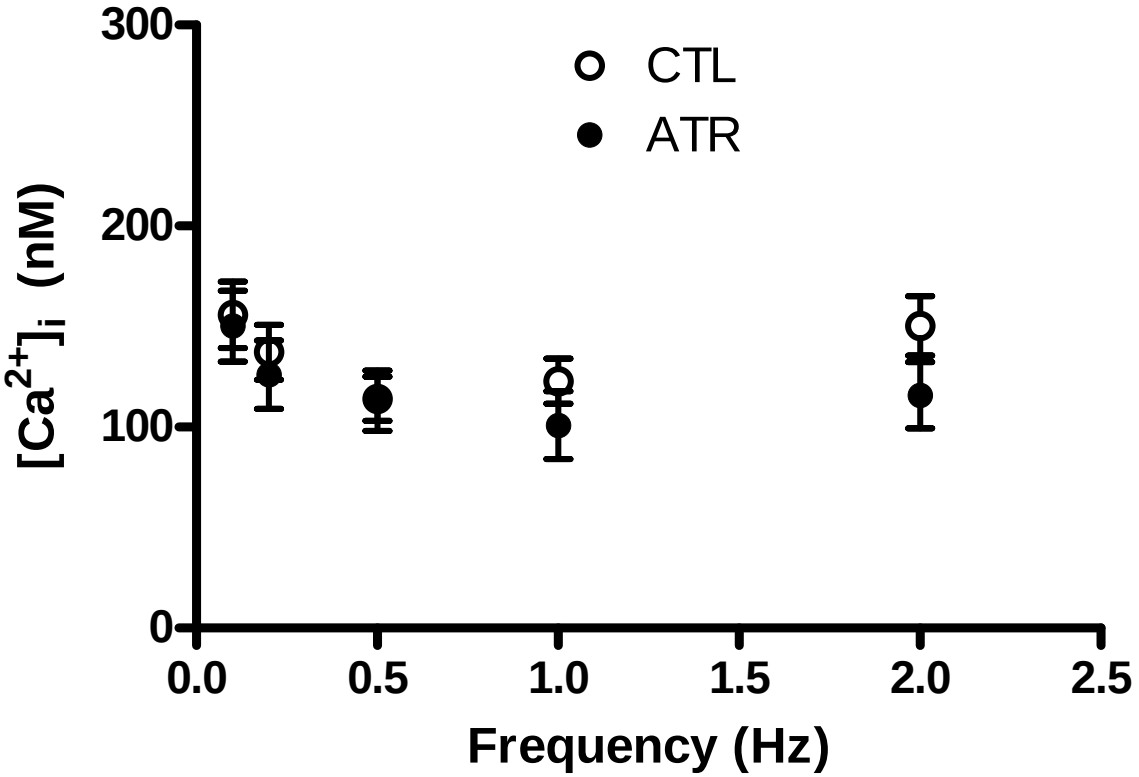

Online Figure 2. Ca^{2+}-transient diastolic levels ATR vs. control (CTL) frequency dependence. Mean±SEM Ca^{2+}-transient diastolic levels in CTL and ATR cardiomyocytes as function of stimulation frequency (n=25, n=15 cells for CTL, ATR; *P*=NS ATR vs. CTL).

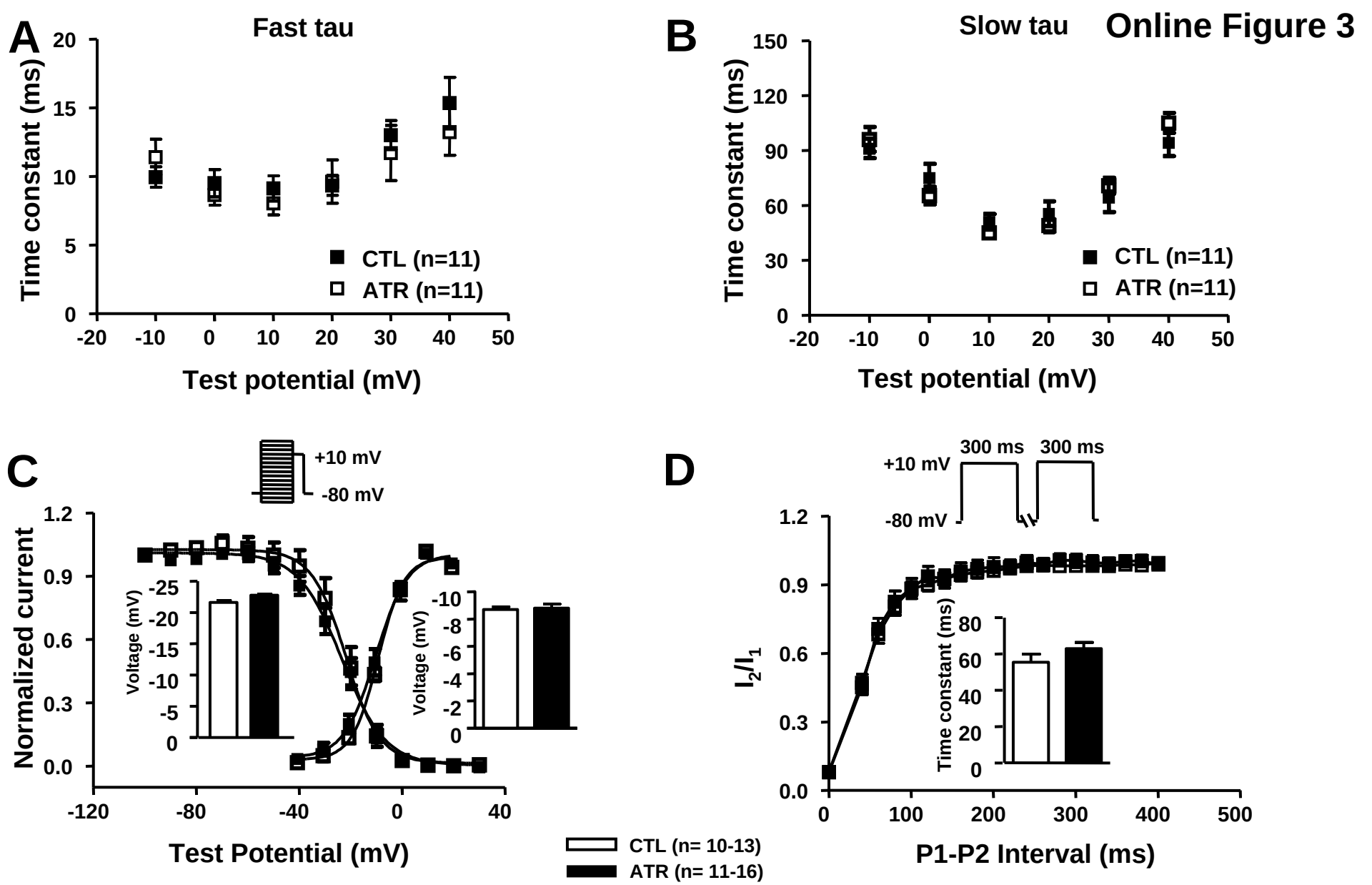

Online Figure 3. Measurements of I_{CaL} with EGTA-containing pipette solution. A,B, I_{CaL} inactivation with EGTA-containing pipette solution; means±SEM, I_{CaL} inactivation time constants tau-fast (A) and tau-slow (B) in control (CTL) and ATR (n=10 cells in CTL, n=16 cells in ATR; **P*<0.05, ***P*<0.01, ATR vs. CTL). C, voltage dependence of I_{CaL} inactivation and activation. Curves are Boltzmann fits to the mean data, insets show corresponding $V_{1/2}$ for inactivation (left) and activation (right). D, I_{CaL} time-dependent recovery; monoexponential fits corresponding to mean data are shown, inset shows time-dependent recovery time-constants.

Online Figure 4

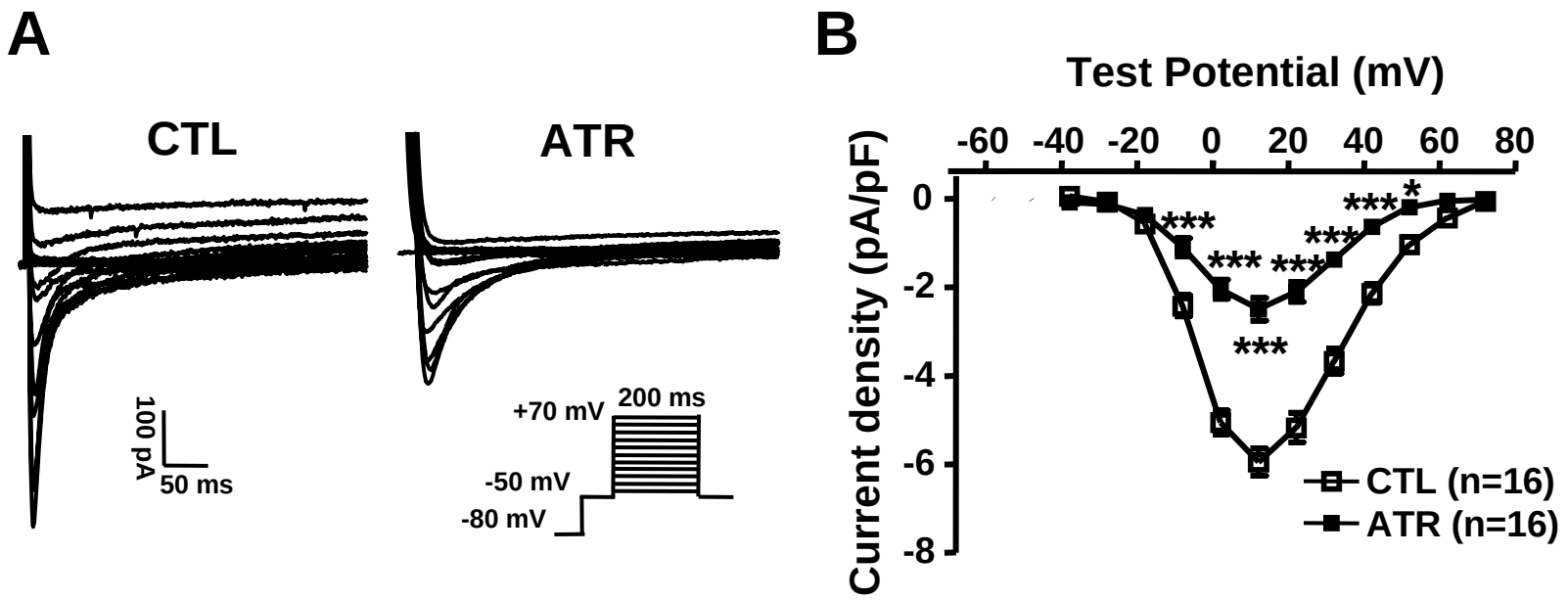

Online Figure 4. EGTA-free measurements of I_{CaL}. **A,** I_{CaL} recordings at 0.1 Hz in control (CTL) and ATR cardiomyocytes with EGTA-free pipette solution; **B**, Mean±SEM I_{CaL} density in CTL and ATR (n=16 cells/group; **P*<0.05, ****P*<0.001, ATR vs. CTL at same test potential).

Online Figure 5

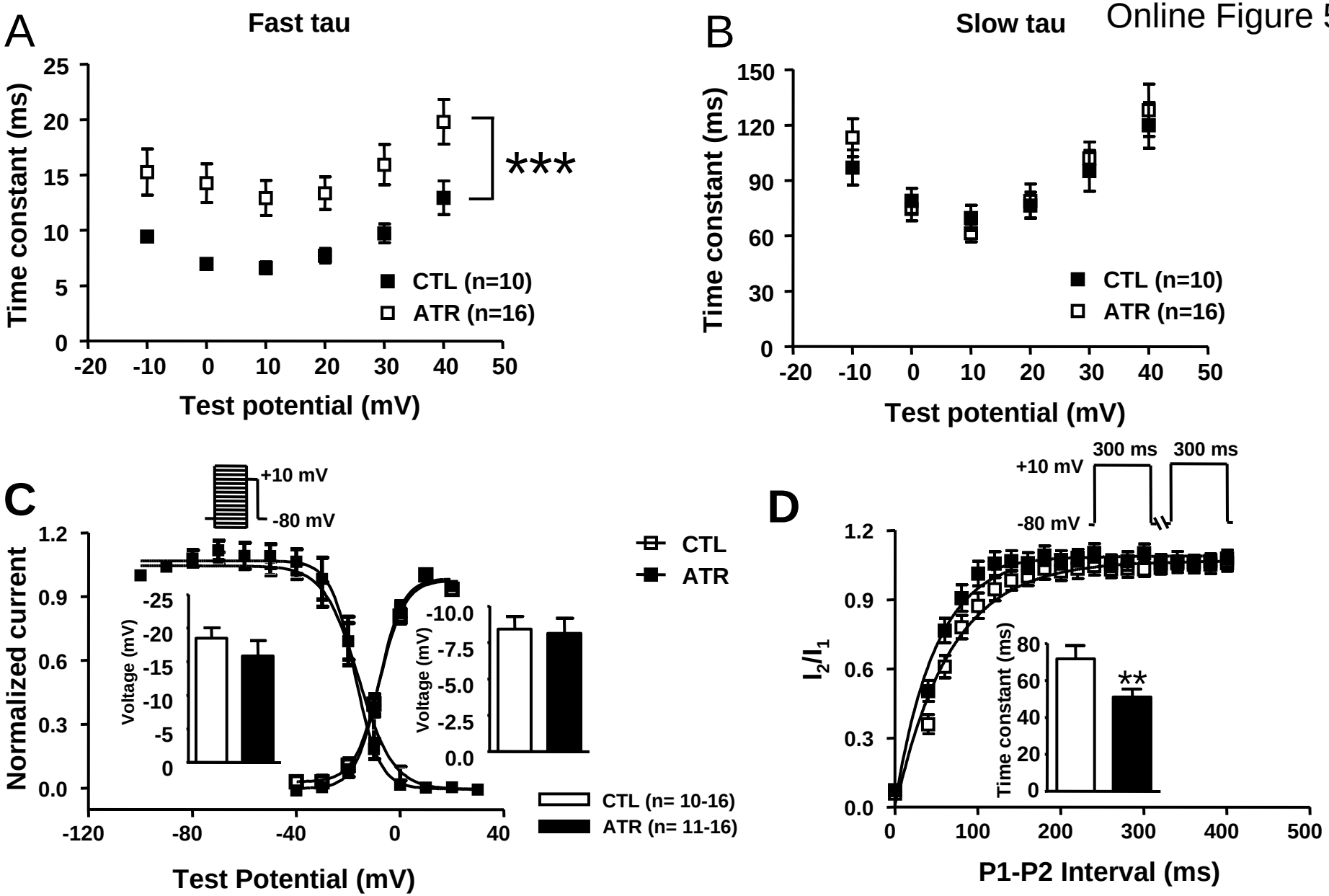

Online Figure 5. A,B, I_{CaL} inactivation with EGTA-free pipette solution; mean±SEM, I_{CaL} inactivation time constants tau-fast (A) and tau-slow (B) in control (CTL) and ATR (n=10 cells in CTL, n=16 cells in ATR; ****P*<0.001, main-effect of ATR vs. CTL). **C,** voltage dependence of I_{CaL} inactivation and activation. Curves are Boltzmann fits to the mean data, insets show corresponding V1/2 for inactivation (left) and activation (right). **D**, I_{CaL} time-dependent recovery; monoexponential fits corresponding to mean data are shown, inset: recovery time-constants, ***P*<0.01.

Online Figure 6

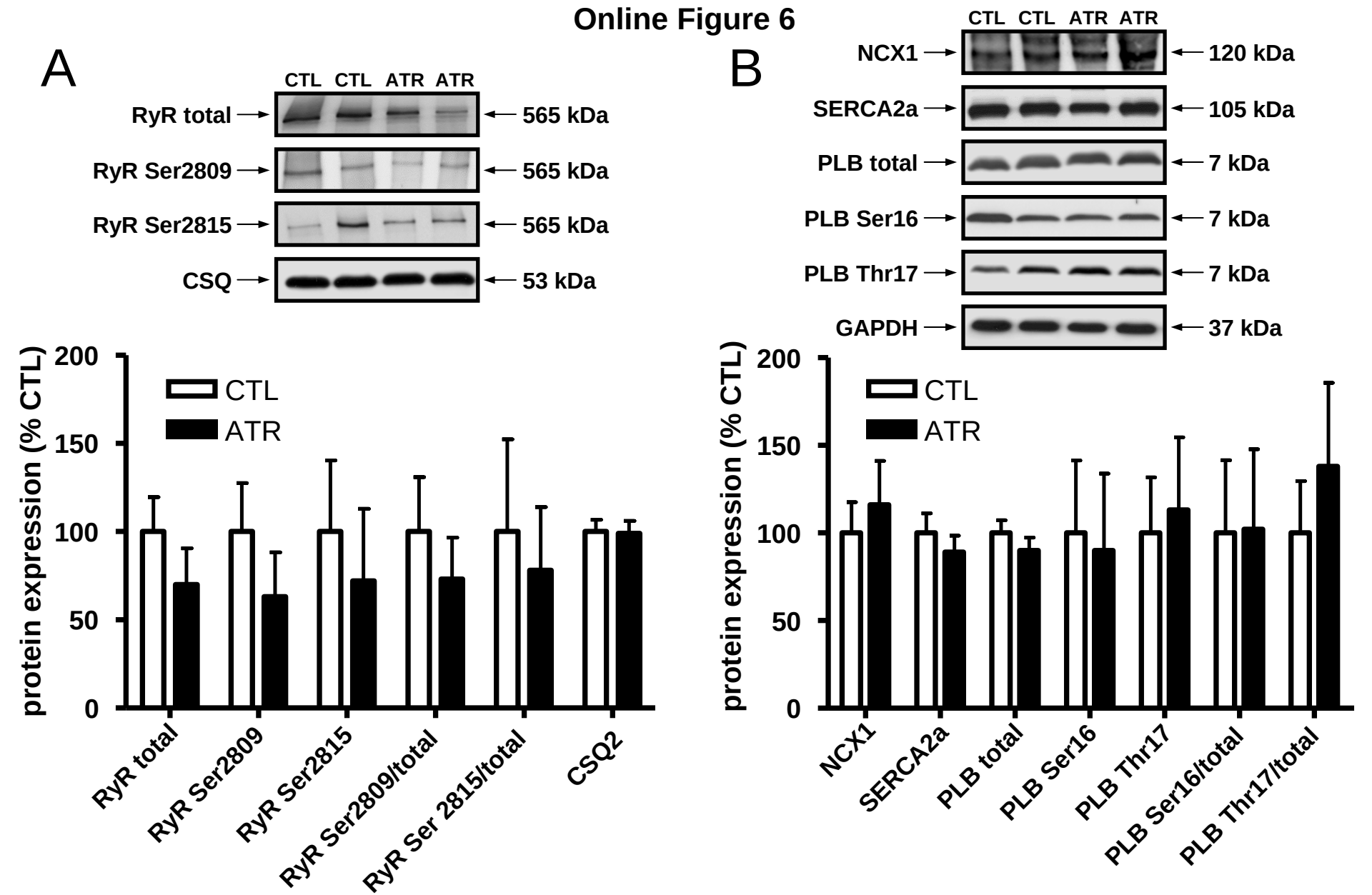

Online Figure 6. A, Top: Immunoblots of total RyR2, Ser2809-P RyR2 and Ser2815-P RyR2, calsequestrin2 (CSQ2) and GAPDH. Bottom: Mean±SEM protein-band intensities of total RyR2, Ser2809-P RyR2 and Ser2815-P RyR2 relative to control (CTL), and CSQ2 normalized to GAPDH, expressed relative to CTL. (n=10 CTL and 7-9 ATR atria for RyR2, and n=14 CTL and 10 ATR for CSQ2; *P*=NS ATR versus CTL). **B**, Top: Immunoblots of NCX1, SERCA2a, total PLB, Ser16-P PLB and Thr17-P PLB and GAPDH. Bottom: Mean±SEM protein-band intensities normalized to GAPDH, relative to control. (n=10 CTL and n=8 ATR atria for NCX1, n=14 CTL and 10 ATR atria/for SERCA and PLB/-P analysis, *P*=NS ATR vs. CTL).

Online Figure 7

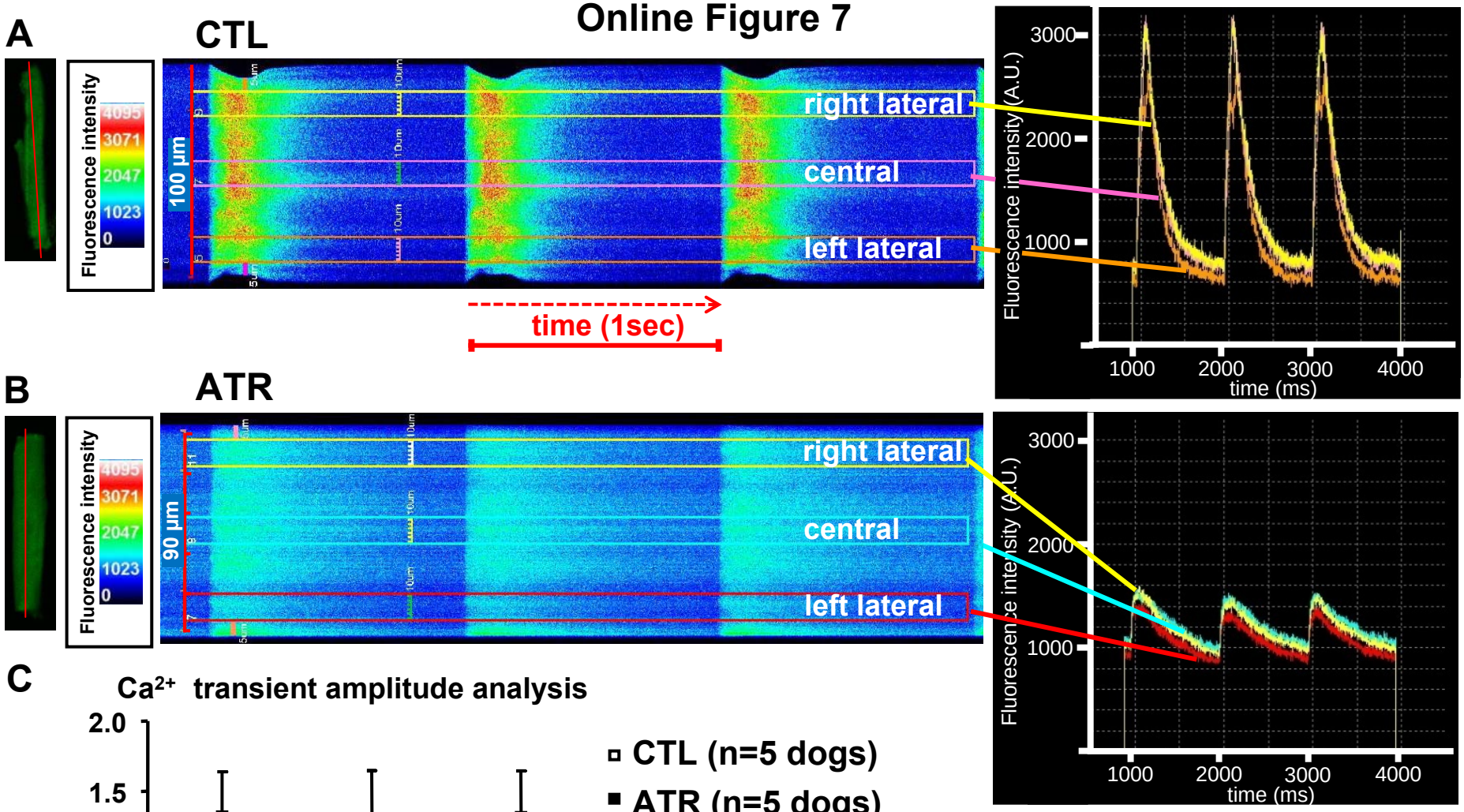

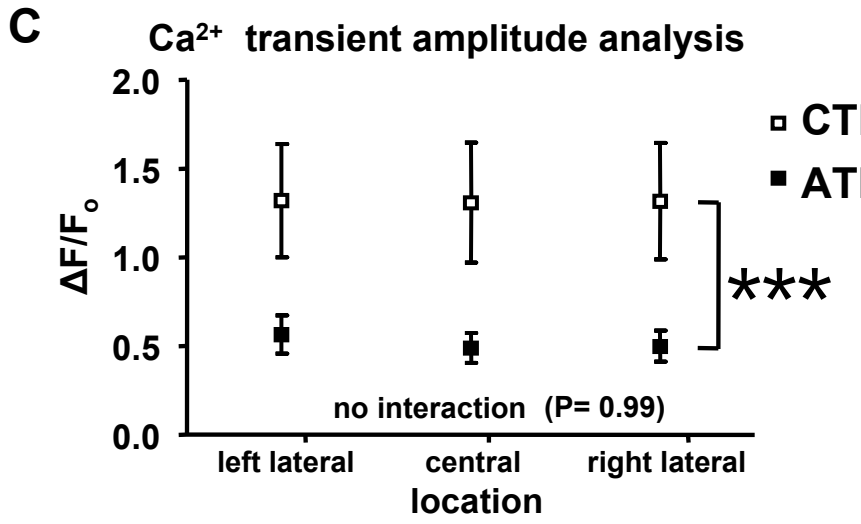

Online Figure 7. Longitudinal spread of Ca^{2+}-fluorescence in control (CTL) and ATR cells. Confocal subcellular Ca^{2+}-transient analysis: **A, B**; representative images showing the cardiomyocyte (left) with the line scan over time (middle) of a control (CTL, **A**) and ATR (**B**) cell; rectangular boxes indicate the regions of interest in the right lateral, central and left lateral part of the cell; the corresponding superimposed Ca^{2+}-transient recordings of each region of interest are shown in the right insets. **C,** Corresponding mean±SEM data for ATR vs. control Ca^{2+}-transient amplitudes in the left lateral, central and right lateral part of the cell (n= 5 dogs/group, *** *P*<0.001 for factor group, ATR vs. control; not significant for factor location; no interaction between the 2 factors).

Online Figure 8

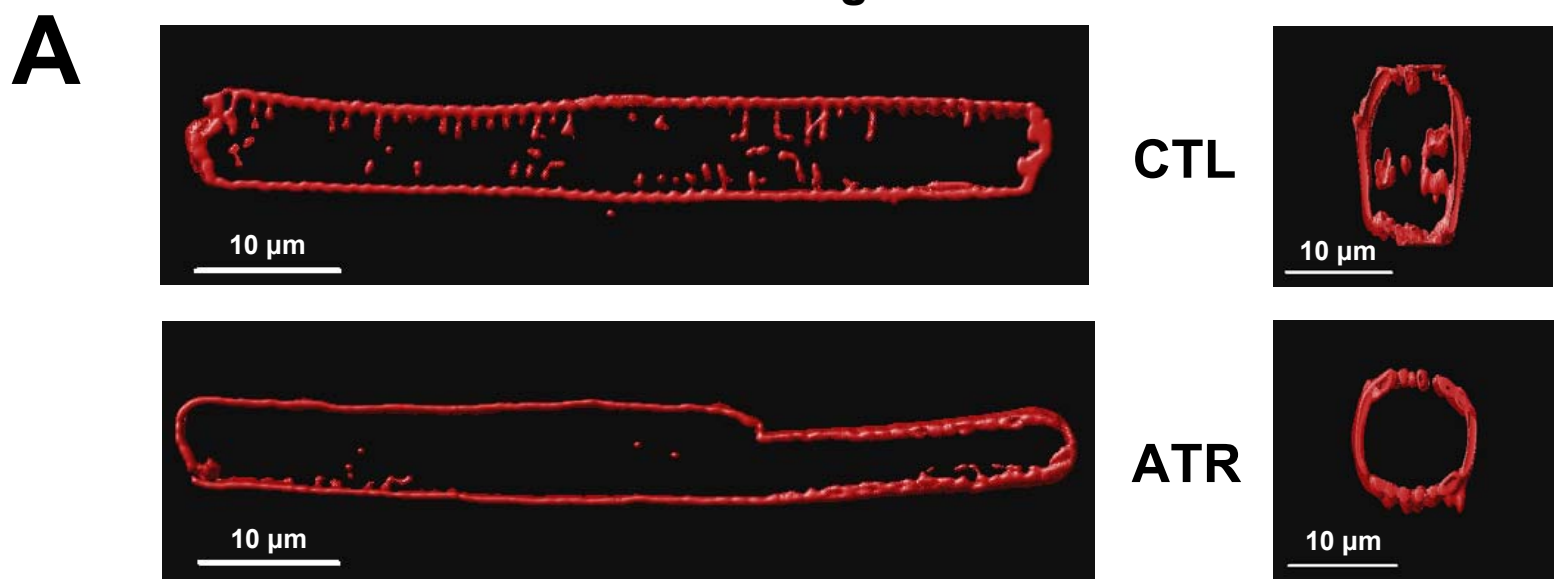

Online Figure 8. A, Examples of di-4-ANEPPS staining in control (CTL) and ATR cardiomyocytes, in longitudinal (left) and transverse (right) views. **B,** T-tubule density calculated by image analysis of non-membrane di-4-ANEPPS staining. ***P*<0.01.

Online Figure 9

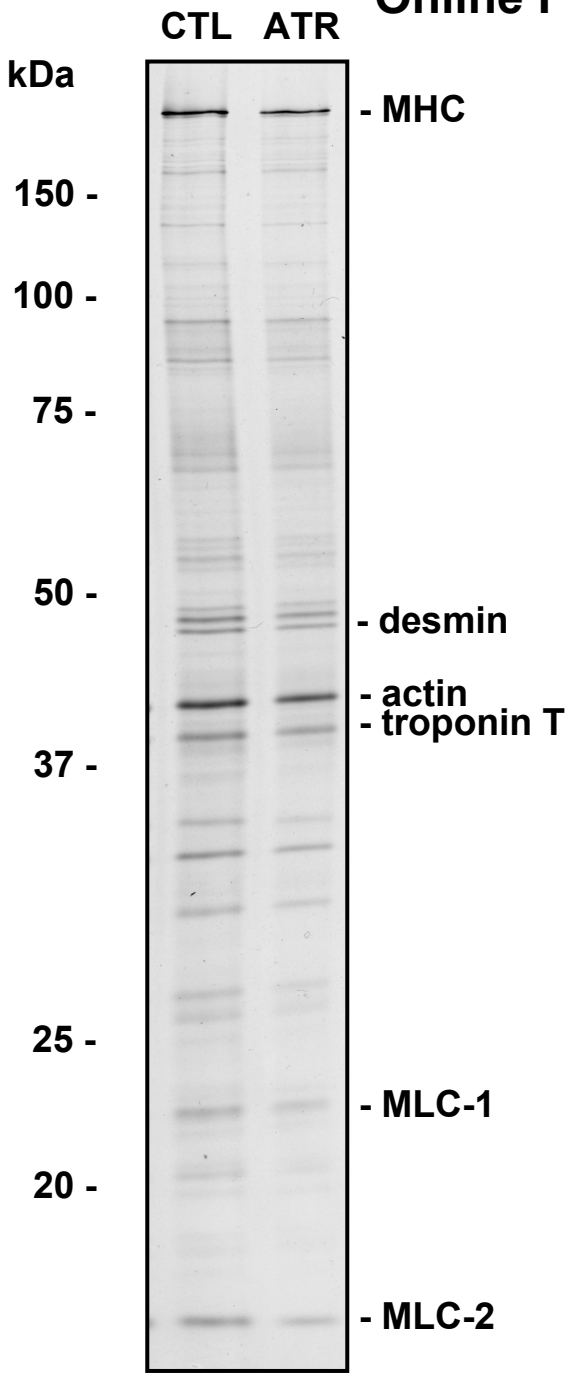

Online Figure 9. Examples of one-dimensional SDS-PAGE gels of control (CTL) and ATR samples determining contractile protein composition.

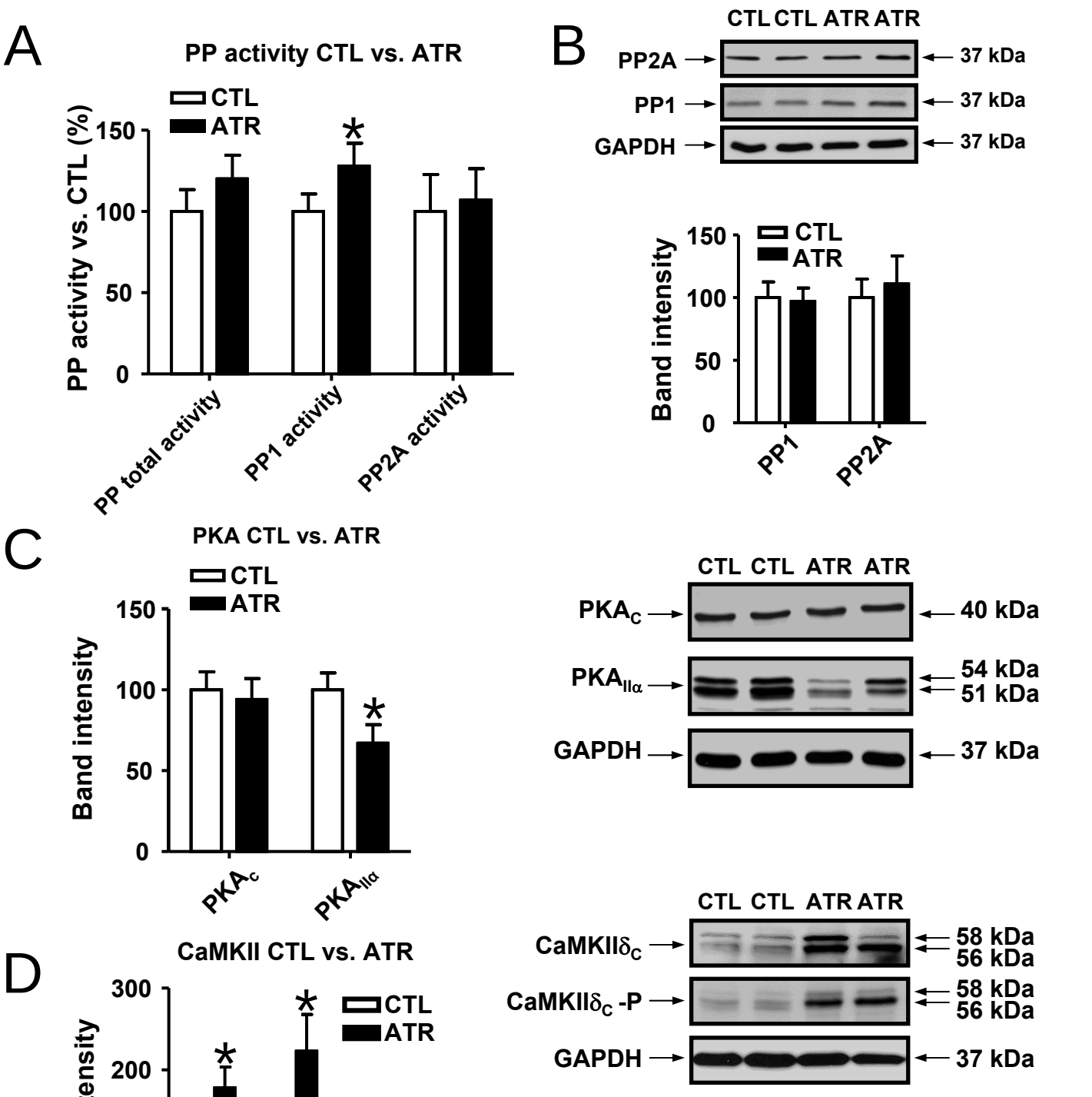

Online Figure 10. **A,** Protein-phosphatase (PP)-activity normalized to control (CTL, n=10 atria per group/analysis, **P*<0.05 vs CTL) and **B,** Corresponding protein-expression. Representative examples (top) and mean±SEM protein-band intensities (bottom). (n=14 CTL /10 ATR for PP1, n=10 CTL/ 8 ATR for PP2A atria/analysis; *P*=NS ATR vs CTL). **C, Right:** Representative immunoblots. PKAIIα bands are at 51 and 54 kDa, quantified as sum of the bands. **Left:** Mean±SEM protein band-intensities. (n=10 CTL, 8 ATR atria/analysis, **P*<0.05 versus CTL). **D**, **Right:** Immunoblots of total CaMKIIδ, Thr-287-phosphorylated CaMKII (autophosphorylated) and GAPDH. Top bands (58 kDa) represent CaMKIIδB, bottom (56 kDa) CaMKIIδC. **Left:** Mean±SEM protein-band intensities. (n=16 CTL, 8 ATR atria/analysis, **P*<0.05 vs CTL). All protein band-intensities are normalized to GAPDH and expressed relative to CTL.

Online Figure 10

Online Figure 11

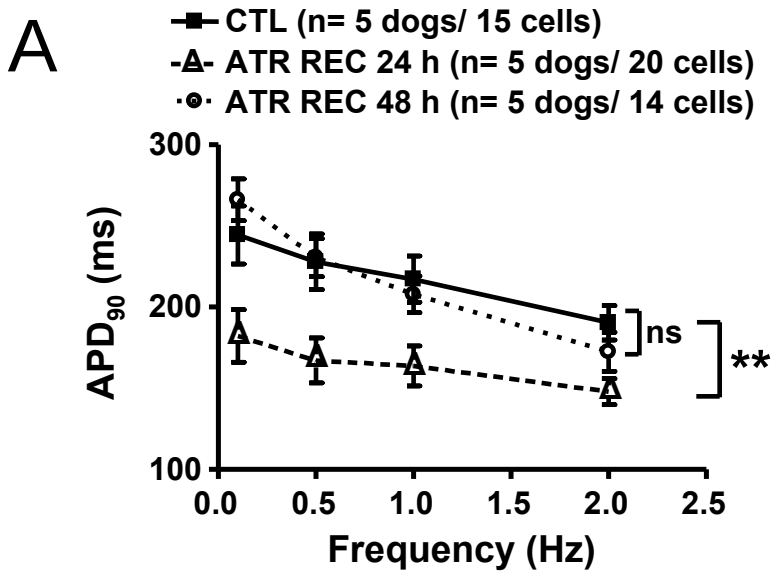

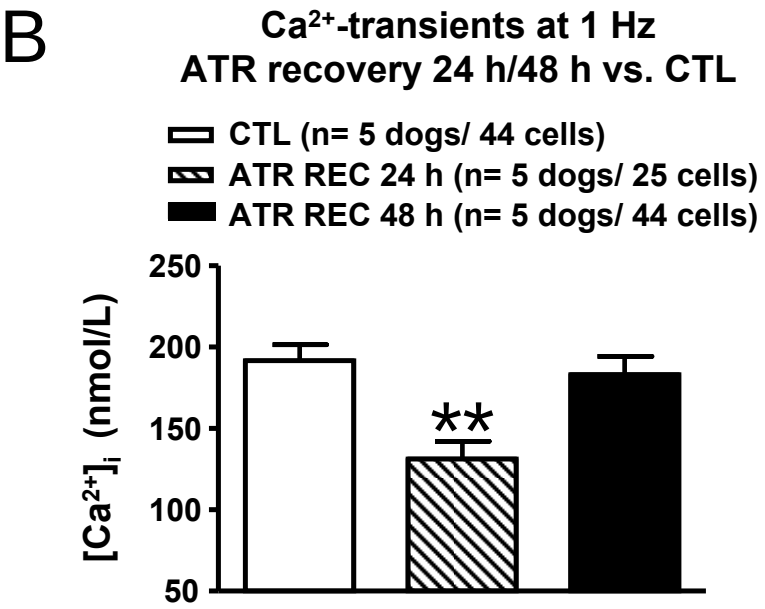

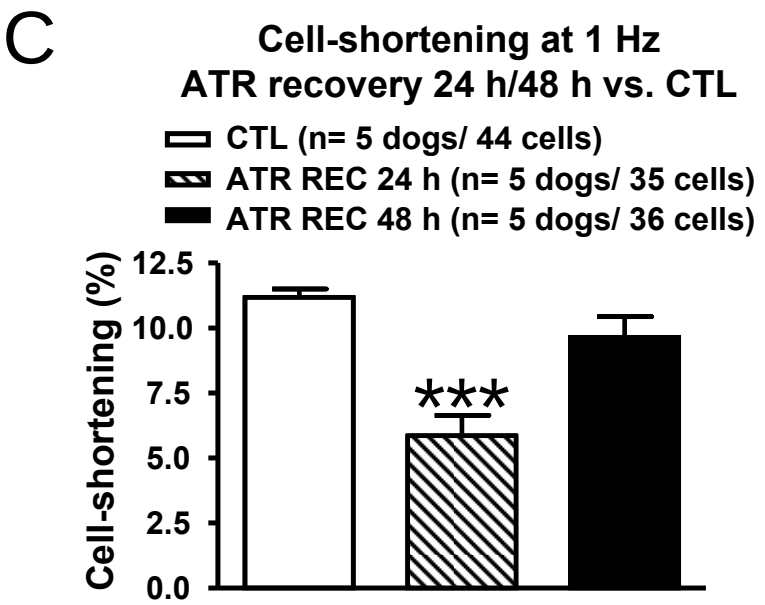

Online Figure 11. Recovery time course of electrophysiological and contractile properties; **A** , Mean±SEM APD_{90} at different frequencies (***P*<0.01, ATR REC 24 h versus CTL, and *P*=NS for ATR REC 48 h versus CTL, effect of group). **B**, Mean±SEM Ca^{2+}-transient amplitude, ***P*<0.01 ATR REC 24 h versus CTL, *P*=NS for ATR REC 48h versus CTL. **C**, Mean±SEM relative cell shortening, ****P*<0.001 ATR REC 24h versus CTL, *P*=NS for ATR REC 48h versus CTL. CTL=control, REC=recovery.